Sea ice, ice-rafting, and ocean climate across Denmark Strait during rapid deglaciation (similar to 16-12 cal ka BP) of the Iceland and East Greenland shelves

Andrews, J. T.; Cabedo-Sanz, P.; Jennings, A. E.; Olafsdottir, S; Belt, S. T.; Geirsdottir, A

Published in:
Journal of Quaternary Science

DOI:
10.1002/jqs.3007

Publication date:
2018

Journal of Quaternary Science

Sea ice, ice-rafting, and ocean climate across Denmark Strait during rapid deglaciation (~16 to 12 cal ka BP) of the Iceland and East Greenland shelves

Journal:	*Journal of Quaternary Science*
Manuscript ID	JQS-17-0023.R2
Wiley - Manuscript type:	Research Article
Date Submitted by the Author:	13-Oct-2017
Complete List of Authors:	Andrews, John; University of Colorado, Arctic and Alpine Research; Cabedo Sanz, Patricia; University of Plymouth, Earth and Environmental Sciences Belt, Simon; University of Plymouth, Petroleum and Environmental Geochemistry Group Jennings, Anne; University of Colorado, INSTAAR Olafsdottir, Saedis; University of Bergen, Department of Earth Science and Bjerknes Centre for Climate Research Geirsdóttir, Áslaug; University of Iceland, Institute of Earth Sciences and Department of Earth Sciences
Keywords:	Denmark Strait, Deglaciation, Ocean reservoir correction, IP25 biomarker, Sedimentology

Sea ice, ice-rafting, and ocean climate across Denmark Strait during rapid deglaciation (~16 to 12 cal ka BP) of the Iceland and East Greenland shelves

Andrews, J.T.[1], Cabedo-Sanz, P.[2], Jennings, A.E. [1], Ólafsdóttir, S[3], Belt, S.T[2], Geirsdóttir, Á.[4]

1. INSTAAR and Department of Geological Sciences, University of Colorado, Boulder, CO 80309, USA

2. School of Geography, Earth and Environmental Sciences, University of Plymouth, Drake Circus, Plymouth, PL4 8AA, UK

3. Department of Earth Science and Bjerknes Centre for Climate Research, University of Bergen, Norway

4. Department of Earth Sciences, University of Iceland, IS-101, Reykjavík, Iceland

JTA: ORCHID 0000-0003-3169-5979

andrewsj@colorado.edu

Abstract

A suite of cores from the Northwest Iceland and East Greenland shelves sampled fossiliferous or unfossiliferous basal glacial diamictons. Radiocarbon dates above the diamictons are similar on both shelves, however, the value of the ocean reservoir correction, ΔR, is unknown. Deglaciation occurred either ~16 or 14 cal ka BP depending on the choice of ΔR. The ice sheets were behind the present coastline by 12.2 cal ka BP. We examine seven cores that record the glacial/deglacial transition and present new data on the sea-ice biomarkers IP_{25} and $C_{25:2}$ from four of the cores plus data on IRD counts, grain-size spectra, $\delta^{18}O$ on the near-surface planktonic foraminifera *Neogloboquadrina pachyderma* (s), foraminifera assemblages, and quartz %. IP_{25} concentrations are markedly higher for the East Greenland sites, while they are frequently below the limit of quantification off Iceland; observations that parallel the wt% quartz in the sediments. The $\delta^{18}O$ *N. pachyderma* (s) data show a strong gradient across Denmark Strait with lighter $\delta^{18}O$ values towards the East Greenland shelf indicative of a large freshwater flux. The presence of the chilled Atlantic Water benthic foraminifera, *Cassidulina neoteretis*, indicates that rapid ice sheet retreat was associated with ocean forcing, combined with other factors.

Keywords: Denmark Strait, Deglaciation, Ocean reservoir correction, IP25 biomarker, Sedimentology
Abstract: 254 words
Main text: 6455 words

Introduction

A significant number of cores from around Iceland and E Greenland penetrate a basal diamicton, often containing shells and foraminifera, overlain by glacial marine sediments rich in ice rafted debris (IRD) (Jennings et al., 2000; Olafsdottir, 2004). At the Late Glacial Maximum (LGM), reconstructions and marine core data (Andrews, 2008; Andrews et al., 1998, 2000; Dunhill, 2005; Funder et al., 2004; Hubbard et al., 2006; Vasskog et al., 2015) indicate that the Iceland and Greenland ice sheets were terminating at their shelf breaks with deposition on the slopes above the Denmark Strait. In a companion paper (Andrews et al., 2017a) we documented the variations of the Iceland and Greenland ice sheets during Marine Isotope Stage (MIS) 3 and LGM as archived in sediments at the northern and southern ends of Denmark Strait. Active sediment deposition ceased on the Kangerlussuaq Trough Mouth Fan ca. 15.3 ka ^{14}C BP (Andrews et al., 1998; Dunhill, 2005) and retreat to the present outer coast occurred prior to deposition of the Vedde tephra (Jennings et al., 2006). Geophysical data from the Kangerlussuaq Trough, E Greenland (Dowdeswell et al., 2010; Stein, 1996), and from the West Iceland shelf (Syvitski et al., 1999) indicate that there are sites where pre Last Glacial Maximum (LGM) sediments exist, but no such sites have been successfully cored. Syvitski et al (1999), Norddahl and Ingolfsson (2015), and Petursson et al. (2015) argued that the Iceland Ice Sheet retreated rapidly driven by a rapid rise in relative sea level. Jennings et al. (2006) presented evidence for a rapid retreat of the Greenland Ice Sheet under the influence of subsurface Atlantic Water from marine cores along Kangerlussuaq Trough (KT, Fig. 1A). Thus evidence for rapid ice retreat has been presented for both the Greenland and Iceland ice sheets citing different reasons for the

retreat and modeling studies of deglaciation (Patton et al., 2017; Tarasov and Peltier, 2002) do not necessarily focus on all multi-proxy evidence. However, in order to understand the forcing mechanism(s) driving ice sheet retreat, the radiocarbon dates have to be adjusted by an ocean reservoir correction that probably varied both temporally and spatially (Stern and Lisiecki, 2013).

The purpose of this paper is to use the paleoceanographic records from sites on either side of the Denmark Strait for the time period between deglaciation and deposition of the Vedde tephra ca 12.1± cal ka BP in order to explore the potential drivers of ice sheet retreat and to test for the synchronicity of Iceland and Greenland ice sheet retreat. Our focus is on determining conditions during deglaciation, and especially the evidence pertaining to the presence of sea ice and icebergs, and whether we can detect evidence for ocean forcing, which may explain some of the differences between field and modeling data (Lecavalier et al., 2014; Sinclair et al., 2016). The cores are from the N Iceland Húnaflói and Djúpáll troughs, and the E Greenland Kangerlussuaq Trough (Fig. 1A, Tables 1 and 2). Although evidence for ice retreat has been presented separately for both the Greenland and Iceland ice sheets, here we examine the combined regional evidence across Denmark Strait using multiple proxy data, with an emphasis on reconstructing deglacial environmental conditions by the use of sea ice biomarkers, foraminifera, light oxygen isotope data, and sediment properties. Biomarker and sediment mineralogy are new here, whereas the other variables have been reported previously. Data from PO175/1-5 (Mienert, 1990) have not been previously published. Of particular interest, given the evidence for present-day ocean warming impacting the retreat of Greenland tidewater glaciers (Andresen et al., 2011, 2012; Holland et al., 2008), is whether the rapid

retreat of the ice sheets in our area can also be attributed to the incursion of Atlantic Water (Jennings et al., 2006; Knudsen et al., 2003) or if there are other important factors. Regardless of the exact chronology (see below) the sequence of events and regional variations will remain intact.

Background to study region

Atlantic Water in the form of the Irminger Current flows as the surface current northward along the West Iceland shelf and splits into two branches, one of which flows eastward along the inner N Iceland shelf, whereas the other branch swings south and is present as an intermediate water mass in the large E and SE Greenland troughs (Fig. 1A) (Andresen et al., 2011; Jennings et al., 2011; Kraus, 1958; Syvitski et al., 1996). On the East Greenland shelf the surface current, the East Greenland Current, consists of a cold, relatively low salinity water mass derived from the Arctic Ocean: the East Iceland Current is a branch of this current (Fig. 1A). Under present conditions there is a pronounced tongue of cold surface water that extends to the east of Iceland (Siedov et al., 2016). Sea ice can be present on the Iceland shelves (Divine and Dick, 2006; Ogilvie, 1992; Ogilvie and Jonsdottir, 2000) bringing in driftwood from Siberia (Eggertsson, 1993; Hellmann and al., 2015), while on the East Greenland shelf sea ice is present for many months of the year (Hastings, 1960). There are no tidewater glaciers on Iceland today whereas on E Greenland there are many tidewater glaciers contributing icebergs onto the inner shelf (Bigg, 1999; Seale et al., 2011).

Our study area lies across the Iceland-Greenland Ridge (Larsen, 1983). Iceland is composed of mid-Tertiary to Recent basalt and other extrusive volcanics (Hardarson et al., 2008), in which the occurrence of quartz and high-pressure feldspars is non-existent

or rare. The occurrence of quartz on the Iceland shelf has been used as an indicator of the incursion of drift ice (i.e. icebergs and sea-ice) (Eiriksson et al., 2000; Moros et al., 2006; Thors, 1974). The bedrock geology on the East Greenland side of Denmark Strait is more complex, with a large (60,000 km^2) outcrop of early Tertiary basalt between Kangerlussuaq Fjord and the southern coast of Scoresby Sund (Brooks and Nielsen, 1982; Brooks, 2008) (Fig. 1A). Cretaceous sandstones and shales exposed in the fjords (Larsen et al., 1999), and Precambrian basement granite gneisses that form most of the hinterland bedrock (Henriksen, 2008), are rich in quartz and k-feldspars which are common components of late Quaternary marine sediments (Andrews et al., 2014, 2015).

Analysis of seafloor surface sediments from the N Iceland shelf indicated that quartz and the sea ice biomarker IP_{25} (Belt et al, 2007) are present and are well correlated with each other, but both are absent in sediments from the W and SW Iceland shelf (Cabedo-Sanz et al., 2016). A paper by Xiao et al. (2017) was recently published on the variations in IP_{25} in core MD99-2272 just to the east of our B997-326 site and at the same site as HM107-05 (Fig. 1).

Methods

The cores (Table 1) were obtained on cruises of the *Poseidon* (1991) (Mienert, 1990), *Jan Mayen* (1996) (Hald, 1996), *Bjarni Sæmundsson* (1997) (Helgadottir, 1997) and *Marion Dufresne* (1999) (Labeyrie et al., 2003). Detailed descriptions of the methods are given as Supplemental Material and the data are available from Pangeae (www.pangeae.de; see Andrews, Cabedo Sanchez, et al., 2017b). Counts of the > 2 mm fraction (Grobe, 1987) are a measure of ice-rafting by icebergs, and the Malvern grain-size spectra (Suppl. Material) also provide evidence on the mode of sediment transport and deposition

(Jonkers et al., 2012). The weight % of quartz on the Iceland Shelf provides a measure of the importation of far-travelled ice-rafted sediments (Andrews, 2009; Eiriksson et al., 2000) whereas calcite wt% is a measure of marine productivity (Thordardottir, 1984, 1986). Regional assessments of oceanographic controls on foraminifera species (Jennings and Helgadottir, 1994; Jennings et al., 2004a; Rytter et al., 2002), stable isotope values (Smith et al., 200; Azetsu-Scott and Tan, 1997), and the sea ice biomarker IP_{25} (Cabedo-Sanz et al., 2016) provide critical information on paleoceanography.

Marine Isotope Stage 2 (MIS2 & 1) radiocarbon dates: INSTAAR Date Lists (Dunhill et al., 2004; Manley and Jennings, 1996; Quillmann et al., 2009; Smith and Licht, 2000; Andrews et al., in prep) contain 82 dates on marine carbonates (shells and foraminfera) ≥ 12.0 ^{14}C ka BP from the region. Additional dates on near surface planktonic foraminifera, benthic foraminifera, molluscs, and mixed benthic and planktonic foraminifera have been obtained from other papers (e.g. Knudsen et al., 2003, 2004)(Suppl. Table 1). Many of the dates noted above and in Supplemental Table 1 were used in the ice sheet modeling study (Patton et al., 2017, see their Table 1). Note that we will refer to the ^{14}C date without marine reservoir correction as "^{14}C ka BP" and the calibrated dates, after correction, as "cal ka BP." We focus on cores that penetrated a basal diamicton or have a robust chronology (Fig. 1, Tables 1 and Suppl. Table 1). We do not attempt to "tune" our data to other records, such as the Renland Ice Cap (Fig. 1A), as such a process can result in circular reasoning (Blaauw, 2012).

^{14}C dates from core tops on the Kangerlussuaq Trough Mouth Fan date ~15 to 16 ^{14}C ka BP (Andrews et al., 1998; Dunhill, 2005) (Fig. 1B) and evidence from NE and W Greenland indicates that the Greenland Ice Sheet started to retreat shortly after the LGM

(O'Cofaigh et al., 2004; Jennings et al., 2017). There are many dates on either side of Denmark Strait range between 12 and 15 ^{14}C ka BP (Fig. 1B) and bracket the dates for deglaciation. Cosmogenic dates on terrestrial outcrops from either side of Denmark Strait (Brynjolfsson et al., 2015; Dyke et al., 2014; Principato et al., 2006; Sinclair et al., 2016), tephra identifications (Andrews et al., 2008; Jennings et al., 2002, 2014), and ^{14}C dates on raised marine deposits (Norðdahl and Ingolfsson, 2015), indicate that the ice sheets retreated to the present coastlines by the time of the Vedde tephra ca 10.6 ^{14}C ka BP (Lecavalier et al., 2014; Lohne et al., 2013). On Figure 1B we plot the basal ^{14}C dates and whether the cores penetrated basal diamictons (Dmm) (Eyles et al., 1983). We also plot the location of cores JM96-1225 and -1228 where the *N. pachyderma* (s) δ^{18}O records (Fig. 2) indicate a rapid decrease of ~1.5‰ from LGM values of ~4.5‰ to 3.5–3‰ (Hagen, 1999a; Hagen and Hald, 2002). The interpolated ^{14}C ages of the δ^{18}O transition in these cores is ~13.9 and 15.6 ^{14}C ka BP. South of our study area the δ^{18}O transition in core DS97-7P (Kuijpers et al., 2003) (63.523°N, -38.658°W, 1843 m wd) is dated at 13.7 ^{14}C ka BP. These rapid changes in the δ^{18}O could be caused by either the input of isotopically light meltwater due to global ice sheet mass loss (Clark et al., 2004; Lambeck et al., 2014; Peltier et al., 2015; Vasskog et al., 2015; Bigg et al., 2011), or by the influx of warm Atlantic Water (Jennings et al., 2006; Knudsen et al., 2003). .

The "unknown" element in establishing a chronology for events is the value(s) for the ocean reservoir correction, ΔR, although the stratigraphic sequence of events in our cores will remain unaltered. There is evidence for variations in ΔR during MIS2 in the northern North Atlantic of up to 1000 yr (Butzin et al., 2005; Sarnthein et al., 2015; Thornalley et al., 2015; Stern and Lisiercki, 2013); however, dates associated with the

Vedde and Saksunarvatn tephras, show that no large-scale ΔR correction is required across the Pleistocene/Holocene transition (Andrews et al., 2002a; Jennings et al., 2002, 2014). Published calibrations have used a ΔR of 0–400 yr (e.g. Jennings et al., 2006; Knudsen et al., 2003; Patton et al., 2017) but we recognize that two alternative arguments can be used to proceed from ^{14}C dates to calibrated dates, and thus we are forced to work within the constraints of a multiple hypothesesis framework (Chamberlin, 1890). Many estimates of larger ΔR's are based on correlations between the marine and Greenland Ice Sheet isotopic records---this requires a close linkage between a climate record from an elevation of ~3 km and a near-surface marine record. The alternative is that the near surface marine δδ^{18}O record was responding to freshwater forcing linked to Heinrich events (Bigg et al., 2011) that is dated ca 17.5 cal ka BP (Bigg, 2016; Bigg et al., 2011). A similar degree of change in δ^{18}O was noted at the H-1 onset in the Labrador Sea (Andrews et al., 1994) associated with a massive freshwater outburst from Hudson Strait (Hesse and Khodabakhsh, 2016). Support for an earlier, hence small ΔR, also comes from the detailed identification of tephras in core PS2644 (Voelker and Haflidason, 2015) (not shown---just north of B997-326 (Fig. 1; 67.866°N, 21.765°W, 777 m wd); the resulting depth/age model indicates that the abrupt δ^{18}O transition in *N. pachyderma* s occurred ~18 cal ka BP.

On Figure 1C (and in Suppl. Table 1) we show the calibrated dates with a ΔR of 0 (we used Oxcal (Bronk Ramsey, 2008)). This results in deglaciation dates of between 15 and 17 cal ka BP and the δ^{18}O transition in JM96-1225 at ~16.2 cal ka BP indicating that deglaciation was coeval with or immediately post-Heinrich event 1 *sensus stricto* (Hemming, 2004; Hesse and Khodabakhsh, 2016). However, given the Greenland ice

cores $\delta^{18}O$ records (Vinther et al., 2008; Rasmussen et al., 2014) and regional marine $\delta^{18}O$ records (Thiagarajan et al., 2014) the abrupt $\delta^{18}O$ decrease in JM96-1225 (Fig. 2) may date from the Bolling/Allerod (B/A) transition at ~14.7 cal ka BP (Rasmussen et al., 2014). If the assumption is made that that the marine $\delta^{18}O$ transition is coeval with is event, then a larger ΔR is required. In order to derive approximate calibrated radiocarbon dates for this second alternative hypothesis we use a ΔR of 1000 ± 200 for dates ~14 ^{14}C ka BP and a ΔR of 0 ± 200 for dates ~10.7 ^{14}C ka BP. We linearly interpolated between these two (ΔR decrease of 303 yr ky^{-1}) in order to obtain a calibrated date. This approach has its limitations, but it serves to provide an internally consistent data set (Suppl. Table 1Table 2). These calibrated basal dates (Fig. 1C,) indicate deglaciation between ~13 and 15 cal ka BP with median age estimates ~13.8 cal ka BP compared to ~15 cal ka BP with a $\Delta R = 0$. For cores MD99-2264 and JM96-1213 we developed depth/age models (Blaauw and Christen, 2011) for the two alternative ΔRs (Suppl. Material and Suppl. Fig. 1).

Results: Core sites and records

We first summarize the analysis of the regional grain-size data and then present these and other proxy data on a core-by-core basis, although the available data are not identical from core to core. Our reporting of the $\delta^{18}O$ on foraminifera is not corrected for vital effects or relative sea level (e.g. Smith et al., 2005). For consistency with earlier papers, we will initially refer to the calibrated dates with $\Delta R = 0$, but with an understanding that these estimates are "less than or equal to." Supplemental. Table 1 contains all calibrated estimates. Data embedded in Figures 3,4, 6 and 7 are archived (www.Pangeae.de).

Grain-size spectra: Sediment grain-size distributions are important indicator of the mode of sediment erosion, transportation, and deposition (Prins et al., 2002; Weltje and Prins, 2007). Rapid retreat of ice sheets and tidewater ice streams is often marked by massive ice-rafted debris (IRD) signal (Andrews, 2000; Bond et al., 1992), but it can also be signaled by meltwater dominated sedimentation (Hesse and Khodabakhsh, 2016).

Grain-size modes (GSMs) (Andrews et al., 2016; Perner et al., 2016) were obtained using k-mean fuzzy clustering (Minasny and McBratney, 2002) on the logratio 42 transformed fractions (Aitchison, 1986)---we did not exclude the coarse sand (IRD component) (Hass, 2002). Fuzzy clustering allows samples to be mixtures of the main GSMs. The degree of mixing, termed the "confusion index (CI)", varies between 0 (a single cluster membership—no confusion) to a maximum of 1. Gradistat data on the samples indicated that many of the samples were polymodal, suggesting transport by more than one process (Curry, 1960). The performance indicators (Fig. 3A) distinguished 3 discrete GSMs. The GSM designations are robust as the confusion index is generally low with only 10% having significant contributions (CI > 0.2) from more than one GSM (Fig. 3B). The average grain-sizes were computed for each of the 3 GSM's (Fig. 3C) and indicate that the majority of the samples (GSM #C, n = 119) are classified as poorly sorted medium silts. The average GSM #A (n = 21, Fig. 3C) is a very poorly sorted, very coarse silt, and the average GSM #B (n = 22) is a coarse silt. A bi-plot of mean grain-size versus sorting supports the 3-fold discrimination of the grain-size spectra, although indicating substantial variability in the range of sorting in GSC #C (Fig. 3D) as does a plot of the percentages of medium sand versus medium silt (Fig. 3E). The samples classified as GSM #C are very poorly sorted with coarser grain-size represent fine-

grained glacial marine diamictons. Ice-rafting of medium and coarser sand is evident in most of the GSM #C as shown by the positive skewness and 500 µm size mode (Figs. 3C and 3F). Additional commentary on the GSMs is reserved for the discussion of the individual core data (below Figs 4, 6 and 7). In these figures under "Lithology" we plot the lithofacies and the descriptive name for the sediment, such as "medium silt," for those sections of the cores where we have grain size data.

North Iceland, Reykjafjarðaáll Trough, core B997-326PC: The Húnaflói/ Reykjafjardaáll Trough (HT, Fig. 1A) provided a bathymetric outlet for a major ice stream that flowed northward to the Iceland Sea (Bourgeois, 2000; Hubbard, 2006; Patton et al., 2017, Principato et al.,2016). Core B997-326PC1 (Fig. 4) lies just south of the average AD 1870-1920 April limit of sea ice (Divine and Dick, 2006) (Fig. 1A). Several cores on the northern limit of the trough (B997 -323, -326) penetrated a matrix supported fossiliferous diamicton (Dmm), with dates between 25 and 44 ^{14}C ka BP (Andrews and Helgadottir, 2003). The contact between the basal diamicton and the overlying glacial marine sediments (Fig. 4) is dated 13,8 ± 0.2 ^{14}C ka BP (16.2 ± 0.3 cal ka BP (Suppl. Table 1). A Borrobol-type basaltic tephra was tentatively identified at 140 cm in B997-326PC2 and correlated with similar tephras just above the basal diamictons in B997-326, -332 and -323 (Andrews and Helgadottir, 2003; see www.noaa.gov/paleo). The Vedde tephra may be present at 125 cm (Andrews and Helgadottir, 2003). A date at 18 cm of 9.7 ± 0.3 cal ka BP indicates that the core either did not recover most of the Holocene or has a compressed Holocene record.

Counts of the > 2mm (IRD) fraction indicate consistent ice-rafting over the interval from ~16 to 9.8 cal ka BP (Fig. 4). Nearly all the grain-size spectra between the

base and 125 cm are classified as GSM #C (Fig. 3) with only two samples classified as #A. The qrtz wt% (≤ 1 %) is much lower than the present-day input (~6 wt%) (Andrews and Eberl, 2007), probably representing the dominance of local quartz-poor sediments. Calcite and total organic carbon (TOC) (Fig. 4) also remain low until the uppermost centimeters, which date from the last 1 cal ka BP (Andrews and Helgadottir, 2003). Although the sea ice biomarker IP_{25} was often present, it was generally not above the limit of quantification. However, the co-occurring sea ice biomarker $C_{25:2}$, is extremely well correlated with IP_{25} on the North Iceland shelf (NIS) (Massé et al., 2011) and could be readily quantified, although its concentration remained low throughout the record.

Foraminifera assemblage data in B997-323, which lies seaward of B997-326 (Fig. 1A), were reported in Andrews and Helgadottir (2003). The core recovered a basal diamicton that extended from the base of the core to 80 cm. The planktonic foraminifera numbers reach values of 100/g during deglaciation and are associated with relatively heavy $\delta^{18}O$ values (3.5–4.0 ‰) (Fig. 10 *in* Andrews and Helgadottir, 2003) suggesting deglaciation occurred early in the glacial/deglacial transition (e.g. Fig. 2). Immediately above the basal diamicton the benthic foraminifera show high percentages (~20%) of the chilled Atlantic Water species *Cassidulina neoteretis* (Jennings and Helgadottir, 1994), indicating that the deglaciation was associated with the incursion of Atlantic Water. Sparse stable isotope data were obtained on $\delta^{18}O$ *N. pachyderma* that showed a sharp increase in $\delta^{18}O$ to 3.8‰ at 60 cm and that Andrews and Helgadottir (2003) tentatively attributed to the Younger Dryas (YD) cold event (12.8 to 11.5 cal ka BP).

NW Iceland, Djúpáll Trough: Djúpáll is a shallow trough (~230 m wd) that extends WNW from Ísafjarðardjúp to Denmark Strait (Fig. 1A). An independent ice cap (Hoppe, 1982;

Norðdahl, 1990) may have existed over NW Iceland and been separated from the main Iceland Ice Sheet during the LGM. A large ridge, interpreted, as a moraine lies seaward of the cores we discuss; the trough contains a large drift deposit (Fig. 5A) (Geirsdóttir et al., 2002; Ólafsdóttir, 2004). Publications on cores from this drift have focused on the last 12 cal ka BP (Andresen et al., 2005; Andrews et al., 2002b, 2013; Ólafsdóttir et al., 2010; Quillmann, 2006; Quillmann et al., 2010). However, several cores in Djúpáll, JM96-1234GC, MD99-2264, and B997-336PC (Andrews et al., 2008; Geirsdóttir et al., 2002), contain ^{14}C dates older than the Vedde tephra (Suppl. Table 1).

Core B997-338PC. This core is situated on the flank of the Djúpáll sediment drift (Fig. 5A). Some of the radiocarbon dates in an initial paper on B997-338PC were incorrect (Andrews et al., 2002b, 2013), probably because of the reworking of foraminifera from the pre-LGM diamicton. The revised chronology is based on two radiocarbon dates on small, articulated shells associated with rhyolithic tephras (Andrews et al., 2013) (Fig. 6A). The two rhyolithic tephras, some 100 cm apart (Suppl. Table 2), might indicate Borrobol-type (BT) tephras (Andrews et al., 2013; Davies et al.,2004; Lind et al., 2016) and thus not in keeping with $\Delta R=0$; however, two rhyolithic tephras were noted in the NGRIP core and dated ~ 15.2 and 15.5 cal ka BP (Mortensen et al., 2005).

The upper 20 cm of core B997-338PC consists of reworked Vedde ash (Fig. 5A) thus consistent with the ^{14}C date of 11.56 ± 0.17 ka BP from 21 cm (Suppl. Table 1). The core (Fig. 6A) consists of a basal diamicton of compacted overridden glacial marine sediments (dry densities of ~1.5 g/cm^3), overlain by poorly sorted, sandy mud or muddy sand (~1 g/cm^3) with some coarse IRD (Chesley, 2005); glacial marine deposition started

~15 cal ka BP. In detail, the GSMs are dominated by #C with an upper interval of #B (Figs. 3 and 6A). The basal diamicton samples are classified as GSM #C, and they comprise the very poorly sorted component (Fig. 3D). Sediment mineralogy is dominated by local basalt sources and the qrtz wt% is very low (<1 %), hence there is little evidence for a contribution by ice-rafting from Achaean/Paleoproterozoic Greenland bedrock. Age estimates ($^{39}Ar/^{40}Ar$) on basalt IRD clasts do, however, indicate that some clasts were derived from the E Greenland early Tertiary outcrop (Principato, 2003; Principato et al., 2006). The sea ice biomarkers IP_{25} and $C_{25:2}$ were generally below the limits of detection, although $C_{25:2}$ could be quantified in a few cases indicating limited occurrence of sea ice.

The modest levels of calcite % (Fig. 6A) indicate there was some marine productivity. The foraminifera consist of sparse planktonic numbers and a fauna dominated by species associated with glacial marine conditions, notably *Cassidulina reniforme* and *Elphidium excavatum* f. *clavata*, which also are the main species in the modern fauna (Jennings et al., 2004a). The chilled Atlantic Water species *C. neoteretis* occurs in low percentages (Fig. 6A). Sparse stable isotope data were obtained on *Cibicides lobatulus*, a common epifaunal species, that occurs in current dominated environments (Jennings et al., 2004b) and which showed $\delta^{18}O$ ratios ~2‰ during deglaciation.

Core MD99-2264 was retrieved from the center of the Djúpáll drift (Geirsdóttir et al., 2002; Olafsdottir, 2004) (Fig. 5A). Estimates of modern (last 2-3 decades) wt% quartz, IP_{25}, and $\delta^{18}O$ *N. pachyderma* (s) were obtained on the accompanying box core MD99-2263 of 2%, 0.004 µg/g, and 2.2‰ respectively (Andrews et al., 2009). The

Vedde tephra was identified at 11.8 m depth. Articulated shells in the basal diamicton Unit A, Fig. 6B) have finite ^{14}C ages of ~53 ka BP, whereas dates above a rhythmite unit (Unit C) range in age between 15.7 and ~12.5 cal ka BP (Figs. 6B). This core has a very high rate of sediment accumulation allowing for unsurpassed detail of events between deglaciation and deposition of the Vedde tephra (Suppl. Fig. 1). Rates of accumulation averaged 200 yr/100 cm or 125 yr/100 cm depending on the chosen ΔR (Suppl. Table 1, Fig. 6B). This, however, does mean that some elements of the record can be diluted especially those we express in percents/g. This core was not included in Patton et al. (2017) paper.

During the initial deglaciation coarse IRD deposition occurred (Fig. 6B, Unit B). The sediment between 11 and 15 m (Unit D) varied between sand to clayey silt, with clay %s between 4 and 23%. Calcite wt% was slightly higher in the diamicton than in the overlying sediment but increases slowly and steadily above 20 m core depth. The same pattern is seen in the wt% of quartz with values usually less than 2% below ~ 16 m. The benthic foraminifera are dominated by the glacial marine Arctic species *C.reniforme* and *E. excavate* f. *clavata* ---these two species are also present in large percentages in the basal diamicton. There are, however, low percentages of the chilled Atlantic Water species *C. neoteretis* as well as the boreal species *C. laevigata,* with a notable but short lived peak in percentages ~1850 cm (~14.5 cal ka BP) suggesting relatively warm conditions (Fig. 6B). Stable $\delta^{18}O$ ratios from the glacial marine sediments ≤ 26 m on the near-surface planktonic foraminifera *N. pachyderma* (s), and on the benthic foraminifera *C. reniforme* (Olafsdottir, 2004) (Fig. 6B) have some outliers. Median $\delta^{18}O$ ratios of 3.0 ‰ and 3.94‰ respectively are intermediate in their values relative to ratios

before and after the B/A transition in Denmark Strait (Hagen, 1999a; Ólafsdóttir, 2004). The large difference between the benthic and planktonic $\delta^{18}O$, especially between 17 and 18 m indicates the presence of a substantial meltwater cap. No IP_{25} or $C_{25:2}$ were detected in samples from 1215 and 1260 cm depth (~12.8 to 13.1 cal ka BP) and coarse IRD is rare above 20 m (~14,3 cal ka BP).

Thus, the 4 basal dates from this area of Iceland range in age between 15.3 - 16.2 cal ka BP ($\Delta R = 0$) versus 13.9 – 14.7 cal ka BP ($\Delta R = \sim 1000$), and present two potentially quite different scenarios in terms of their glaciological interpretation(s).

East Greenland: Kangerlussuaq Trough is a deep cross-shelf trough that trends nearly N-S from Kangerlussuaq Fjord to the shelf break south of Denmark Strait (Dowdeswell et al., 2010; Mienert et al., 1992; Stein, 1996). Stein (1996) mapped a series of recessional moraines along the Trough (Fig. 1A).

Core PO175/1-5 is a 3.2 m long core collected from 501 m water (Mienert, 1990), thus from a depth generally below the limit for iceberg scouring (Syvitski et al., 2001). A series of short gravity cores were also collected nearby in ~300 m of water and record conditions over the last ca. 150 yr, including both sediment mineralogy and IP_{25} abundance (Alonso-Garcia et al., 2013). The seismic record across PO175/1-5 (Stein, 1996) sampled Unit L of Stein (Fig. 5B). The radiocarbon dates indicate that the bulk of the sediment was deposited between ~17 and 15 ^{14}C ka BP (Fig. 7A), although the dates show some reversals, probably from reworking of earlier glacial marine sediments (Suppl. Fig. 1). No grain-size data are available.

The quartz and calcite wt% are relatively constant throughout (Fig. 7A) but the quartz is less than 50% of the wt% recorded for recent decades in PO176/GKC 9 (Alonso-Garcia et al., 2013), whereas the wt% of calcite has a median value of 0.5% versus 3.3 % in PO176/GKC 9 (i.e. modern). The relatively low quartz wt% indicates that the sediment was predominantly derived from erosion of the E. Greenland early Tertiary basalt outcrop (Andrews et al., 2015). The foraminifera data show fluctuating numbers/g for both the benthic and planktonic species. What is especially noticeable, given the link with cooled Atlantic Water (Jennings and Helgadottir, 1994), is the presence of *C. neoteretis,* which peaks between 150 and 60 cm, whereas the glacial marine species of *C. reniforme* and *E. excavatum* occur in relatively constant percentages although higher in the early part of the record. The $\delta^{18}O$ data on the near-surface planktonic species *N. pachyderma* (s) showed relatively little variation about a median value of 2.8‰.

Both sea ice biomarkers (IP_{25} and $C_{25:2}$) show similar trends (Fig. 7A), with low concentration ~300–140 cm depth, after which, values showed an increasing, but variable trend between ~140–60 cm. At 40 cm, a reduction in IP_{25} and $C_{25:2}$ concentrations coincided with a decrease in the quartz data, although there is a generally poor relationship between the biomarkers and quartz wt%. Highest IP_{25} and $C_{25:2}$ concentrations were observed during the YD (~25 cm), before returning to lower concentrations towards the top of the core.

JM96-1213GC is a 540 cm long core that was retrieved in 557 m of water in the inner/mid- section of the deep Kangerlussuaq Trough (Hald, 1996)(Fig. 1A and 5C). The lithofacies consist of two intervals of diamicton with high IRD, counts and two units

of fine-grained "wispy" laminated muds (Fig. 7B); the basal diamicton (Dmm) is interpreted as a till (Jennings et al., 2002). Four radiocarbon dates were obtained between the top of the diamicton and the Vedde tephra at ~100 cm (Jennings et al., 2002) (Fig.7B; Suppl. Table 1). The two basal deglaciation dates from cores in the Kangerlussuaq Trough range in age between ~17.6 and 16.2 cal ka BP ($\Delta R = 0$) as opposed to 14.7 to 15.8 cal ka BP with the variable ΔR (Suppl. Table 1 and Suppl. Fig. 1: Fig. 7B).

The GSM modes show cohesive sequences that partly mimic the lithofacies. The basal diamicton and another at ~350 cm are classified as GSM #B and (Fig. 3 and 7B), although this mode is not restricted to the Dmm facies, but frequently it coincides with increased IRD input. The YD interval is marked by a marked light $\delta^{18}O$ peak in the polar species *N. pachyderma* (s) (Jennings et al., 2006) and a switch to GSMs #C and A (Figs. 3 & 7B). The qXRD analysis indicated that calcite was close to the detection limit throughout (< 1%) whereas quartz had limited variability around a median wt% of 4.7 with a maximum of 7%. The mineralogy is dominated by pyroxene and plagioclase indicating glacial erosion and transport from the nearby early Tertiary basalt outcrop (Andrews et al., 2015).

The biomarker data exhibit a generally different trend to that of quartz wt%, although both are lowest below ~420 cm depth (Fig. 7B). Thus, an alternating profile in IP_{25} and $C_{25:2}$, with lowest values during the YD and a peak ~80 cm (Fig. 7B), are not observed in the quartz profile, which exhibits a general increase above ~420 cm.

Discussion

We know little about the stability of the regional ice streams prior to the LGM, although inferences have been made based on nearby deep-sea marine records (Andrews et al., 1998; Hagen and Hald, 2002; van Kreveld et al., 2000). The basal deglaciation dates on cores across Denmark Strait suggest a near synchronous retreat of the Iceland and the East Greenland ice sheets across their respective shelves, although the precise timing is ambiguous because of the uncertainty in ΔR. Estimates of the rate of retreat from the E Greenland shelf break to Kangerlussuaq Fjord depend on which ocean reservoir correction is used, but in both N Iceland and E. Greenland the ice sheets were back to the present coastline by ~12.2 cal ka BP (e.g. Patton et al., 2017).

The geochemistry of the rhyolithic tephras in B997-338 (Andrews et al., 2013) closely matches those of the Borrobol tephra (Suppl. Table 2). On the N Iceland shelf, Gudmundsson et al (2012) identified a "Borrobol-like" tephra in MD99-2272 and attached an age to it of 14.5 cal ka BP; this identification was used in the Xiao et al (2017) paper. The similarity coefficient (Sarna-Wojckicki et al., 1984) between the B997-338 tephras and the geochemistry of the type Borrobol (Lind et al., 2016) suggests the closest match with the geochemistry at 90 cm. If correct, this supports the larger ΔR age estimates. Borrobol-like tephras have not yet been noted from the Kangerlussuaq Trough and in our N Iceland cores the basaltic tephras (Suppl. Table 2) are more difficult to assign to a specific source (Gudmundsson et al., 2012). If the larger ΔR correction is correct, and the evidence points toward that conclusion, then the rate of retreat along the Kangerlussuaq Trough (Fig. 1A) approached ~200 m/yr and are comparable with recent changes in Greenland ice streams (Khan et al., 2014).

There is strong evidence that a major change in deep-water circulation at ~15 cal ka BP resulted in abrupt warming at the onset of the Bølling/Allerød (B/A) interstadial (Thiagarajan et al., 2014; Thornalley et al., 2011). This transition is recognized as a "tipping point" (Turney et al., 2016) in the Northern Hemisphere's climate system (Praetorious and Mix, 2014, 2016) and it is also marked by an abrupt decrease in the $\delta^{18}O$ of precipitation falling on both the NGRIP site and the nearby Renland Ice Cap (Vinther et al., 2008)(Fig 1A). However, we cannot be absolutely certain that this atmospheric-derived event was coeval with the abrupt decrease in the $\delta^{18}O$ of *N. pachyderma* (s) in Denmark Strait (Fig. 2), which might rather reflect surface ocean response to freshwater inputs (Bigg et al., 2011),

or forcing by atmospheric CO_2 variations (Marcott et al., 2014). Glaciological modeling of the retreat histories of the Greenland and Iceland ice sheets have to consider appropriate calibrated age data and for both ice sheets the fall-back position is to use $\Delta R = 0$ (e..g. Tarasov and Peltier, 2002; Patton et al., 2017).

Time dependent processes that influence ice sheet stability include changes in relative sea level, insolation, and ocean warming. On Figure 8A we plot the median calibrated ages and their 95% age range for the two alternative ΔR's for the deglaciation, and the median dates for the two alternative ΔR corrections (Fig. 8B). Note that the Patton et al. (2017) paper used a ΔR of 24 ± 23 yr, so their modeled retreats match our $\Delta R = 0$ chronology, and the Sinclair et al (2016) paper also used a $\Delta R = 0$. The difference of ~1.5 cal ky between the two possible chronologies is most marked at a critical time that would place initial deglaciation close to 16 versus ~14.5 cal ka BP (Figs. 6B and 7B). Between 20 and 12 cal ka BP global sea level rose by nearly 60 m

(Lambeck et al., 2014) (Fig. 8C) but rates of change varied dramatically (Fig. 8D). Summer insolation at 65°N rose steadily over this period (Fig. 8E). Syvitski et al (1999) and Norðdahl and Ingólfsson (2015) questioned whether the retreat of the Iceland Ice Sheet could have been driven by the increase in sea level associated with deglaciation (Clark et al., 2002)--- rapid increases in sea level occurred at ~17 and ~15 cal ka BP (Fig. 8D). The argument that rapid deglaciation is associated with relative sea level changes, driven by glacial isostasy and eustasy, is not new (e.g. Hughes, 2011; Tanner, 1965) and has been invoked as an Heinrich event mechanism (Andrews, 1998). However, the local relative sea level (RSL) requires knowledge of the rate of glacial isostatic recovery, which away from the coast (i.e. observations) must be modeled (Peltier et al., 2015; Roy and Peltier, 2015). Models of RSL for our area (Fig. 8C) indicate that glacial isostatic recovery would have resulted in a modest decrease of water depth at ice fronts.

Sinclair et al. (2016) suggested that some of the discrepancy between modeling of the post-LGM history of the GIS and field observations, including E Greenland (Lecavalier et al., 2014), might be due to the lack of ocean forcing in the ice sheet models. On Figure 9 we compare our proxies from the deglaciation to ~12 cal ka BP, and note, where available, the present-day values from our surface/core top samples, and on Figure 10 we illustrate our conclusions in the form of a simplified 3-part scenario. Specific conditions during deglaciation (Figs. 4, 6 and 7) included: 1) significant amounts of coarse > 2 mm IRD during deglaciation indicating a flux of debris-ladened icebergs, 2) variable sea ice conditions at the East Greenland sites compared to relatively infrequent drift ice occurrence on the N Iceland shelf (as indicated by low sea ice biomarker and qrtz wt%)---both drift ice proxies are lower than late Holocene values

(Cabedo-Sanz et al., 2016) (Fig. 9C & F), 3) the presence of *C. neoteretis* (Fig. 9E) indicates that ice retreat was associated with the incursion of Atlantic Water, 4) $\delta^{18}O$ values of *N. pachyderma* (s), significantly lighter than during the LGM and a noticeable E to W trend in the *N. pachyderma* (s) $\delta^{18}O$ signal (Fig. 9D), and 5) significantly higher percentages of calcite off N Iceland.

In our cores the evidence for a distinct YD event is not dramatic, although there is an increase in $\delta^{18}O$ in B997-323 and -322 (Fig. 4) whereas on the E Greenland shelf the YD is marked by a distinct light $\delta^{18}O$ signal (Jennings et al., 2006). The YD might also marked by erosional intervals in Djúpáll (Fig. 4, 5, 6 and 7) and be indicated by the increase in quartz and k-feldspar and by the large difference in benthic versus planktonic $\delta^{18}O$ of 2.93‰ in MD99-2264 (Ólafsdóttir 2004), suggestive of a meltwater cap. In this core the grain-size data show that silt and clay % increased between ~12.7–12.2 cal ka BP whereas the sand fraction increased to 70-90% from ~12.2–11.8 cal ka BP. In JM96-1213GC (Fig. 7B) both sea ice biomarkers decrease to non-detectable values during the YD, which suggests either a lack of sea ice or extensive (perennial) landfast sea ice (Figs. 9C and 10). In a number of other Arctic/sub-arctic records, the YD is often characterized by significantly elevated IP_{25} abundances (Cabedo-Sanz et al., 2013; Müller et al., 2014; Belt et al., 2015; Méheust et al., 2016); however, ice conditions are somewhat different for the East Greenland sites, insofar as drift ice delivery can be impeded by the presence of near-permanent thick landfast sea ice, such that reduced sea ice biomarker content may be associated with the latter conditions (e.g., Alonso-Garcia et al., 2013). In contrast, higher IP_{25} (and $C_{25:2}$) abundances during the BA and Preboreal periods (e.g., Fig 7B) potentially reflect reduced landfast ice cover with increased drift ice reaching the cores

sites (Alonso-Garcia et al., 2013). Such an explanation cannot be used to account for the low/absent IP_{25} content for the N Iceland sites, however, which presumably reflects limited sea ice conditions overall (Fig. 10). In any case, despite the strength of the $\delta^{18}O$ YD signal on the Greenland Ice Sheet (Alley, 2000) the YD cold period (GS 1) is not a striking event in our marine cores.

Our study and conclusions are based on a broad geographic coverage of sites (Fig. 1 and 10) and multi-proxies, but is focused on the area around Denmark Strait. However, a recent biomarker-based study of sea ice conditions, also on the North Icelandic Shelf but further north and east of our core sites, provides further context to our findings. Thus, Xiao et al. (2017) analyzed IP_{25} and phytoplankton biomarkers in a core (MD99-2272) located ca. 67°N; 18°W, concluding that sea ice conditions were extensive during the Bolling-Allerod, more seasonal during the YD and absent during the early Holocene. Unfortunately, deglacial conditions were not reported from this core. However, differences with our own findings, especially during the Bolling-Allerod and YD, likely reflect the contrasting nature of the sea ice conditions apparent in each study. Specifically, our proxy data almost certainly reflect drift ice conditions (by comparison with modern analogue signatures of biomarkers and qtz content), while the data of Xiao et al. (2017) are interpreted in terms of local biomarker production and thus indicative of a retreating seasonal sea ice margin as observed in many previous IP_{25}-based sea ice reconstructions (e.g., Belt et al., 2015; Berben et al., 2017; Hörner et al., 2016; Müller et al., 2009, 2012; Müller and Stein, 2014; Stein et al., 2017). Common to both studies, however, are generally reduced sea ice conditions during the YD compared to the Bolling-Allerod. Interestingly, the data of Xiao et al. (2017) show a return in IP_{25} content

during the mid-Holocene – starting ca. 6.5 cal ka BP – a feature that has been reported previously from an additional core from the same study site (JR51-GC35) and another core located slightly further west (MD99-2269; ca. 66.38°N; 20.51°W) (Cabedo-Sanz et al., 2016), both of which were interpreted as reflecting changes to drift ice conditions, especially as IP_{25} content had previously been shown to be well correlated with observational sea ice records from the region (Massé et al., 2008). Indeed, the presence of IP_{25} in MD99-2272 during the mid-Holocene (Xiao et al., 2017) is accompanied by increased phytoplankton biomarker content, which contrasts the Bolling-Allerod and YD profiles where high IP_{25} is accompanied by relatively low phytoplankton biomarker concentrations, a combination consistent with extensive spring sea ice cover (Belt and Müller, 2013; Belt et al., 2015; Berben et al., 2017; Hörner et al., 2016; Müller et al., 2009, 2012; Müller and Stein, 2014; Stein et al., 2017. As such, the IP_{25} data in MD99-2272 likely reflect a shift from local seasonal sea ice occurrence during the Bolling-Allerod and YD to drift ice in the Holocene. Although confirmation of the former is challenging due to absence of any modern analogue for the study region, the various studies highlight significant localized sensitivity with respect to sea ice conditions post-deglaciation.

Conclusions

Figure 10 presents a visual capsule of ice sheet extent and ocean surface conditions for the LGM, initial deglaciation, and the YD. Specific points are:

- Uncertainty in the ΔR correction represents a major limitation in establishing detailed regional marine-based correlations.

- Detailed search for, and geochemical fingerprinting of tephras > 11 and < 15 ^{14}C ka BP would potentially resolve the ΔR uncertainty, especially the identification , if present, of the Borrobol tephra and ^{14}C dating of associated sediments. Tephra data from B997-338 points toward the use of a large ΔR in calibrating deglaciation dates.
- The use of the Greenland Ice Sheet's isotopic records as a 1: 1 template for coeval changes in glacier and ocean response potentially ignores the different response time-scales between the atmosphere, oceans, and cryosphere.
- Deglaciation of the shelves on either side of Denmark Strait was rapid, probably starting ~15 (or ~17) cal ka BP with ice margins on the outer coasts by Younger Dryas time.
- Deglaciation was initiated by the incursion of Atlantic Water and aided by a combination of bathymetry and changes in relative sea level.
- Biomarker, stable isotope, and mineral proxies indicate that differing conditions prevailed on the N Iceland versus E Greenland shelves during deglaciation and the YD with more drift ice on the East Greenland shelf.
- Further changes in sea ice conditions are evident further east with a general temporal shift from seasonal local sea ice to absent or drift ice conditions during the Holocene.
- Evidence for a return to glacial conditions during the YD cold event is sparse and complex in our marine archives.

Acknowledgements

The research of JTA and AEJ has been supported by several former NSF grants. The contributions from the other authors has been supported by a RANNIS Grant of Excellence #141573-052: ANATILS: Integrating paleoclimate reconstructions with modeling to understand abrupt climate change in the northern North Atlantic awarded to A. Geirsdóttir & G.H. Miller. JTA thanks his colleague Dennis Eberl for his help and instructions over the years of using quantitative mineral identification via XRD. We thank the editor and reviewers for their helpful comments on previous drafts of this manuscript, which have served to clarify both text, tables, and figures.

The authors confirm that there is no conflict of interest in the submission and content of this manuscript.

Tables

Table 1: Core locations---latitude, longitude, and water depth. Available proxies for the six cores are also listed. Note that because of space on Fig. 1C not all sites could be plotted.

Suppl. Table 1: Radiocarbon dates, errors and calibrated ages

Suppl. Table 2: Geochemical data from cores B997-338, --326, and -323 and comparison with the Lipari obsidian standard (Hunt and Hill, 1996)

Figure captions

Figure 1A: Map of the Denmark Strait area showing the primary cores (solid squares), cores noted in the text and providing information (filled stars; Suppl.Table 1). Dotted blue line = average position of the sea ice edge (15% coverage) April AD 1870-1920 (Divine and Dick, 2006). KT = Kangerlussuaq Trough, H = Húnaflói, the Djúpáll Trough is located at core MD99-2264. Surface Atlantic Currents: Irminger Current = IC, North Iceland Irminger Current (NIIC); cold surface Arctic/Polar Currents: East Greenland Current = EC, East Iceland Current = EIC. B) Map of basal uncorrected ^{14}C dates and whether the core penetrated a basal diamicton (Dmm). Black squares show the two cores with stable isotope records across the glacial/deglacial transition. C) The calibrated ^{14}C dates with values based on a ΔR of 0 versus the sliding scale ΔR estimates (Table 2). The number in brackets along Kangerlussuaq Fjord (11.8 cal ka BP) is the average cosmogenic date (Dyke et al., 2014).

Figure 2: *Neogloboquadrina pachyderma* s δ^{18}O records from north and south of Denmark Strait (Hagen, 1999) illustrating the transition from glacial to interstadial values, and the differences in the radiocarbon dates that we assume is associated with regional variations in the ocean reservoir correction (see text).

Figure 3: Analysis of the grain-size spectra. A) Plot of the 3 performance indictors in FuzMe (Minansy, 2010; Minasny and McBratney, 2002) (MPE= modified partition entropy, FPI = fuzziness performance indicator, S = Compactness and separation validity function) indicating the optimal solution of 4 Grain-size mode (GSM) clusters; B) Probability plot of the Confusion Index (CI) (0 = certainty of cluster membership, 1 = equal mixture of the 3 grain-size modes C) Plot of the average grain-size spectra for the 3

GSMs; D) Plot of the mean grain-size (μm) and sorting; E) Plot of the percentages of medium sand versus medium silt; and F) Plot of aspects of the shape of the grain-size spectra, Skewness versus Kurtosis (Folk and Ward, 1957; Blott and Pye, 2001).

Figure 4: Downcore plots of data from B997-326 and -323 (Fig. 1) on the N Iceland shelf (see Tables 1 and 2) for available data and radiocarbon dates. Data are on percentage values unless otherwise noted. Stable isotope data (δ^{18}O NPs) for *N. pachyderma* (s). Red dashed lines show the possible location of basaltic tephras and solid red lines (also Figures 6 and 7) show the position of rhyolithic tephras (T). The calibrated dates from B997-323 are listed as (cal ka 323).

Figure 5: A) Seismic (chirper) plot across the Djúpáll Drift (Geirsdottir et al., 2002; Olafsdottir, 2004). The insert shows the bathymetry and location of the cross-section. B) Seismic section along the outer Kangerlussuaq Trough showing the relative location of the sites for BS1191-K18B/JM96-1216 and 175PO/1-5 in unit L (from Stein, 1996). C) Seismic stratigraphy at the site of JM96-1213GC.

Figure 6A & B: Downcore plots of data from the Djupal Trough, NW Iceland (Fig. 1) A) B997-338 showing the location of the rhyolithic tephras (red dashed lines) and calibrated dates ΔR = 0. B) MD99-2264. The depth/age plots show the models for a ΔR = 0 in blue and the variable ΔR in red—the Vedde tephra is indicated by the red dashed line. The vertical dashed line shows depth of the ~14.5 cal ka BP for either model. The δ^{18}O data are for *C. reniforme* (benthic) (Cr) and *N. pachyderma* (s) (planktonic)(Nps). The plot (B- P ‰) shows the δ^{18}O difference between the benthic and planktonic paired measurements.

Figure 7A and B: Downcore plots of cores from the Kangerlussuaq Trough (Fig. 1A, Table 1) A) PO175/1-5, and B) JM96-1213. The depth/age plots show the models for a $\Delta R = 0$ in blue and the variable ΔR in red—the Vedde tephra is indicated by the red dashed line. The vertical dashed line shows depth of the ~14.5 cal ka BP for either model. The $\delta^{18}O$ data are on the near-surface planktonic foraminifera *N. pachyderma* (s).

Figure 8: Global and regional parameters operating in the period between 12 and 17 cal ka BP. A) Plot of median calibrated ages and the 95% confidence interval for sites discussed in this paper (Fig. 1, see Table 2) using $\Delta R = 0$ (red) and $\Delta R \leq 1000$ yr (blue). The vertical solid blue and red lines represent the median ages for the basal dates for the two ΔR options; C) Eustatic sea level (Lambeck et al., 2014) and estimates of relative sea level change (RSL) at specific latitudes and longitudes (Peltier, person. commun. 2016). D) Rate of change of global sea level (C); and E) July Insolation at 65°N (Berger and Loutre, 1991);

Figure 9: Box plots of surface & near-surface environment proxies across Denmark Strait (east to west) between 12 to ~15 cal ka BP--- –numbers give the wt% of modern samples showing: A) Weight % quartz; B) Weight % calcite; and C) IP25; D) $\delta^{18}O$ for the near-surface polar planktonic foraminifera *Neogloboquadrina pachyderma*; E) Map of the % of *C. neoteretis* for the deglacial interval > 12 cal ka BP; F) Diene II.

Figure 10: Simplified scenarios of conditions in Denmark Strait at the end of MIS2 and during the initial period of deglaciation. Red triangles represent icebergs and the white patches represent sea ice. Black dots refer to the core locations as listed in Table 1. Red arrows represent warm surface (Atlantic Water) currents and the dark blue represents the

686 export of cold Polar Water. A) Ice Sheet extent during the LGM; B) conditions during
687 deglaciation, and C) Conditions at the YD interval.
688

References

Aitchison, J., 1986. The statistical analysis of compositional data. Chapman and Hall, London, 416 pp.

Alley, R.B., 2000. The Younger Dryas cold interval as viewed from central Greenland. Quaternary Science Reviews 19, 213-226.

Alonso-Garcia, M., JT, A., Belt, S.T., Cabedo-Sanz, P., Darby, D., Jaeger, J., 2013. A multi-proxy and multi-decadal record (to AD 1850) of environmental conditions on the East Greenland shelf (~66°N). The Holocene 23, 1672-1683.

Andresen, C.S., Bond, G., Kuijpers, A., Knutz, P., Bjorck, S., 2005. Holocene climate variability at multi-decadal time-scales detected by sedimentological indicators in a shelf core NW off Iceland. Marine Geology 214, 323-338.

Andresen, C.S., McCarthy, D.J., Dylmer, C.V., Seidenkrantz, M.S., Kuijpers, A., Lloyd, J.M., 2011. Interaction between subsurface ocean waters and calving of the Jakobshavn Isbrae during the late Holocene. Holocene 21, 211-224.

Andresen, C.S., Straneo, F., Ribergaard, M.H., Bjork, A.A., Andersen, T.J., Kuijpers, A., Norgaard-Pedersen, N., Kjaer, K.H., Schjoth, F., Weckstrom, K., Ahlstrom, A.P., 2012. Rapid response of Helheim Glacier in Greenland to climate variability over the past century. Nature Geoscience 5, 37-41.

Andrews, J.T., 1998. Abrupt changes (Heinrich events) in late Quaternary North Atlantic marine envrionments: a history and review of data and concepts. Journal of Quaternary Science 13, 3-16.

Andrews, J.T., 2008. The role of the Iceland Ice Sheet in sediment delivery to the North Atlantic during the late Quaternary: how important was it? Evidence from the area of Denmark Strait. Journal of Quaternary Science 23`, 3-20.

Andrews, J.T., 2009. Seeking a Holocene drift ice proxy: non-clay mineral variations from the SW to N-central Iceland shelf: trends, regime shifts, and periodicities. Journal of Quaternary Science 24, 664-676.

Andrews, J.T., Belt, S.T., Olafsdottir, S., Masse, G., Vare, L., 2009. Sea ice and marine climate variability for NW Iceland/Denmark Strait over the last 2000 cal. yr BP. The Holocene 19, 775-784.

Andrews, J.T., Bigg, G.R., Wilton, D.J., 2014. Holocene sediment transport from the glaciated margin of East/Northeast Greenland (67-80°N) to the N Iceland shelves: Detecting and modeling changing sediment sources Quaternary Science Reviews 91, 204-217.

Andrews, J.T., Bjork, A.A., Eberl, D.D., Jennings, A.E., Verplanck, E.P., 2015. Significant differences in late Quaternary bedrock erosion and transportation: East versus West Greenland ~ 70°N and the evolution of glacial landscapes. Journal of Quaternary Science 30, 452-463.

Andrews, J.T., Cabedo Sanchez, P., Jennings, A.E., Olafsdottir, S., Belt, S.T., Geirsdottir, A., 2017b. Data supplement to: Sea ice, ice-rafting, and ocean climate across Denmark Strait during rapid deglaciation (~16 to 12 cal ka BP) of the Iceland and East Greenland shelves, http://www.pangeae.de.

Andrews, J.T., Cooper, T.A., Jennings, A.E., Stein, A.B., Erlenkeuser, H., 1998. Late Quaternary iceberg-rafted detritus events on the Denmark Strait/Southeast Greenland continental slope (~65° N): Related to North Atlantic Heinrich Events? . Marine Geology 149, 211-228.

Andrews, J.T., Dunhill, G., Vogt, C., Voelker, A., 2017a. Denmark Strait during the LGM and MIS3: sediment transport processes and sources: an examination of a D-O hypothesis Marine Geology 390, 181-198.

Andrews, J.T., Eberl, D.D., 2007. Quantitative mineralogy of surface sediments on the Iceland shelf, and application to down-core studies of Holocene ice-rafted sediments. Journal of Sedimentary Research 77, 469-479.

Andrews, J.T., Erlenkeuser, H., Tedesco, K., Aksu, A., Jull, A.J.T., 1994. Late Quaternary (Stage 2 and 3) Meltwater and Heinrich events, NW Labrador Sea. Quaternary Research 41, 26-34.

Andrews, J.T., Geirsdottir, A., Hardardottir, J., Principato, S., Gronvold, K., Kristjansdottir, G.B., Helgadottir, G., Drexler, J., Sveinbjornsdottir, A., 2002a. Distribution, sediment magnetism, and geochemistry of the Saksunarvatn (10180 60 ± cal

yr BP) tephra in marine, lake, and terrestrial sediments, NW Iceland. Journal of Quaternary Science 17, 731-745.

Andrews, J.T., Hardarddottir, J., Helgadottir, G., Jennings, A.E., Geirsdottir, A., Sveinbjornsdottir, A.E., Schoolfield, S., Kristjansdottir, G.B., Smith, L.M., Thors, K., Syvitski, J.P.M., 2000. The N and W Iceland Shelf: Insights into Last Glacial Maximum Ice Extent and Deglaciation based on Acoustic Stratigraphy and Basal Radiocarbon AMS dates. Quaternary Science Reviews 19, 619-631.

Andrews, J.T., Hardardottir, J., Geirsdottir, A., Helgadottir, G., 2002b. Late Quaternary ice extent and depositional history from the Djupall trough, off the Vestfirdir peninsula, north-west Iceland: A stacked 36 cal environmental record. Polar Research 21, 211-226.

Andrews, J.T., Hardardottir, J., Stoner, J.S., Mann, M.E., Kristjansdottir, G.B., Koc, N., 2003. Decadal to millennial-scale periodicities in North Iceland shelf sediments over the last 12,000 cal yrs: long-term North Atlantic oceanographic variability and Solar forcing. Earth and Planetary Science Letters 210, 453-465.

Andrews, J.T., Hardardottir, J., Stoner, J., Principato, S.M., Geirsdottir, A., 2008. Holocene sediment magnetic properties along a transect from Isafjardardjup to Djupall, Northwest Iceland. Arctic, Antarctic, and Alpine Research 40, 1-14.

Andrews, J.T., Helgadottir, G., 2003. Late Quaternary ice cap extent and deglaciation of Hunafloaall, NorthWest Iceland: Evidence from marine cores. Arctic, Antarctic, and Alpine Research 35, 218-232.

Andrews, J.T., Jennings, A.E., Coleman, C.G., Eberl, D., 2010. Holocene variations in mineral and grain-size composition along the East Greenland glaciated margin (ca 67-70°N): local versus long-distant sediment transport. Quaternary Science Reviews 29, 2619-2632.

Andrews, J.T., Stein, R., Moros, M., Perner, K., 2016. Late Quaternary changes in sediment composition in NE Greenland Fjords, Shelf, Slope, and Deep Sea. Boreas 45, 381-397.

Andrews, J.T., Vogt, C., 2014a. Results of Bulk Sediment X-ray Diffraction Analysis and Quantification of Mineral Phases Based on the RockJock and on the QUAX Quantita-tive Analysis. http://dx.doi.org/10.1594/PANGAEA.830397. doi:10.1594/PANGAEA.830395.

Andrews, J.T., Vogt, C., 2014b. Source to Sink: Statistical identification of regional variations in the mineralogy of surface sediments in the western Nordic Seas (58°N – 75°N; 10° W -- 40°W)). Marine Geology 357, 151-162.

Austin, W.E.N., Wilson, L.J., Hunt, J.B., 2004. The age and chronostratigraphical significance of North Atlantic Ash Zone II. Journal of Quaternary Science 19, 137-146.

Azetsu-Scott, K., Tan, F.C., 1997. Oxygen Isotope Studies from Iceland to an East Greenland Fjord: Behavior of Glacial Meltwater Plume. Marine Chemistry 56, 239-251.

Belt, S.T., Cabedo-Sanz, P., Smik, L., Navarro-Rodriguez, A., Berben, S.M.P., Knies, J., Husum, K., 2015. Identification of paleo Arctic winter sea ice limits and the marginal ice zone: optimised biomarker-based reconstructions of late Quaternary Arctic sea ice. Earth and Planetary Science Letters 431, 127–139.

Belt, S.T., Masse, G., Rowland, S.J., Poulin, M., Michel, C., and LeBlanc, B. 2007. A novel chemical fossil of palaeo sea ice: IP25. Organic Gechemistry 38: 16-27.

Berben, S.M.P., Husum, K., Navarro-Rodriguez, A., Belt, S.T., Aagaard-Sørensen, S., 2017. Semi-quantitative reconstruction of early to late Holocene spring and summer sea ice conditions in the northern Barents Sea. Journal of Quaternary Science.

Berger, A., Loutre, M.F., 1991. Insolation values of the climate of the last 10 Million years. Quaternary Science Reviews 10, 297-318.

Bigg, G.R., 1999. An estimate of the flux of iceberg calving from Greenland. Arctic, Antarctic, and Alpine Research 31, 174-178.

Bigg, G.R., 2016. Icebergs. Their Science and links to Global Change. Cambridge University Press.

Bigg, G.R., Levine, R.C., Green, C.L., 2011. Modelling abrupt glacial North Atalntic freshening: Rates of change and their implication for Heinrich events. Global and Planetary Change 79, 176-192.

Blaauw, M., 2012. Out of tune: the dangers of aligning proxy archives. Quaternary Science Reviews 36, 38-49.

Blaauw, M., Christen, J.A., 2011. Flexible Paleoclimate Age-Depth Models Using an Autoregressive Gamma Process. Bayesian Analysis 6, 457-474.

Blott, S.J., Pye, K., 2001. GRADISTAT: A grain size distribution and statistics package for the analysis of unconsolidated sediments. Earth Surface Processes and Landforms 26, 1237-1248.

Bond, G., Heinrich, H., Broecker, W.S., Labeyrie, L., McManus, J., Andrews, J.T., Huon, S., Jantschik, R., Clasen, S., Simet, C., Tedesco, K., KLas, M., Bonani, G., Ivy, S., 1992. Evidence for massive discharges of icebergs into the glacial Northern Atlantic. Nature 360, 245-249.

Bourgeois, O., Dauteil, O., Van Viet-Lanoe, B., 2000. Geothermal control on ice stream formation: flow patterns of the Icelandic Ice Sheet at the Last Glacial Maximum. Earth Surface Processes and Landforms 25, 59-76.

Bronk Ramsey, C., 2008. Deposition models for chronological records. Quaternary Science Reviews 27, 42-60.

Brooks, C.K., Nielsen, T.F.D., 1982. The Phanerozoic development of the Kangerdlugssuaq area, East Greenland. Meddelelser on Gronland, Geoscience 9, 1-30.

Brooks, K., 2008. A new geologiocal map of East Greenland. Geology Today 24, 28-30.

Brynjolfsson, S., Schomacker, A., Ingolfsson, O., Keiding, J.K., 2015. Cosmogenic Cl-36 exposure ages reveal a 9.3 ka BP glacier advance and the Late Weichselian-Early Holocene glacial history of the Drangajokull region, northwest Iceland. Quaternary Science Reviews 126, 140-157.

Butzin, M., Prange, M., Lohmann, G., 2005. Radiocarbon simulations for the glacial ocean: The effects of wind stress, Southern Ocean sea ice and Heinrich events. Earth and Planetary Science Letters 235, 45-61.

Cabedo-Sanz, P., Belt, S.T., Jennings, A.E., Andrews, J.T., Geirsdottir, A., 2016. Variability in drift ice export from the Arctic Ocean to the North Icelandic Shelf over the last 8,000 years: a multi-proxy evaluation. Quaternary Science Reviews.

Castaneda, I.S., Smith, M.L., Kristjansdottir, G.B., Andrews, J.T., 2004. Temporal changes in Holocene del18O records from the northwest and central North Iceland Shelf. Journal of Quaternary Science 19, 1-14.

Chamberlin, T.C., 1890. The Method of Multiple Working Hyptheses. Science 15, 754-759.

Chesley, T., 2005. Mineralogy, sediment, and foraminiferal history of Djupall, Iceland: reconstructing a past record, Department of Geological Sciences. University of Colorado, Boulder, p. 62.

Clark, P.U., M., M., Mix, A.C., Weaver, A.J., 2004. Rapid rise of sea level 19,000 years ago and its global implications. Science 304, 1141-1144.

Clark, P.U., Mitrovica, J.X., Milne, G.A., Tamisiea, M.E., 2002. Sea-level fingerprinting as a direct test for the source of Global Meltwater Pulse 1A. Science 295, 2438-2441.

Cook, A.J., Holland, P.R., Meredith, M.P., Murray, T., Luckman, A., Vaughan, D.G., 2016. Ocean forcing of glacier retreat in the western Antarctic Peninsula. Science 353, 283-286.

Curray, J.R., 1960. Tracing sediment masses by grain size modes, 21st International Geological Congress, Cophenhagen, pp. 119-130.

Davies, S.M., Wohlfarth, B., Wastegard, S., Andersson, M., Blockley, S., Possnert, G., 2004. Were there two Borrobol Tephras during the early Lateglacial period: implications for tephrochronology? Quaternary Science Reviews 23, 581-589.

Divine, D.V., Dick, C., 2006. Historical variability of the sea ice edge position in the Nordic Seas. Journal of Geophysical Research 111, 1 of 14, doi:10.1029/2004JC002851.

Dowdeswell, J.A., Evans, J., Cofaigh, C.O., 2010. Submarine landforms and shallow acoustic stratigraphy of a 400 km-long fjord-shelf-slope transect, Kangerlussuaq margin, East Greenland. Quaternary Science Reviews 29, 3359-3369.

Dunhill, G., 2005. Iceland and Greenland margins: A comparison of depositional processes under differnt glaciological and oceanographic settings, Geological Sciences. University of Colorado, Boulder, p. 242.

Dunhill, G., Andrews, J.T., Kristjansdottir, G.B., 2004. Radiocarbon Date List X: Baffin Bay, Baffin Island, Iceland, Labrador, and the northern North Atlantic. Occasional Paper No. 56, Institute of Arctic and Alpine Research, UNiversity of Colorado, Boulder, 77 pp.

Dyke, L.M., Hughes, A.L.C., Murray, T., Hiemstra, J.F., Andresen, C.S., Rodes, A., 2014. Evidence for the asynchronous retreat of large outlet glaciers in southeast Greenland at the end of the last glaciation. Quaternary Science Reviews 99, 244-259.

.Eggertsson, O., 1993. Origin of the driftwood on the coasts of Iceland: A dendrochronological study. Jokull 43, 15-32.

Eiriksson, J., Knudsen, K.L., Haflidason, H., Henriksen, P., 2000. Late-glacial and Holocene paleoceanography of the North Iceland Shelf. Journal of Quaternary Science 15, 23-42.

Eyles, C.H., Eyles, N., Miall, A.D., 1983. Lithofacies types and vertical profile models; an alternative approach to the description and environmental interpretation of glacial diamict and diamictite sequences. Sedimentology 30, 393-410.

Folk, R.K., Ward, W.C., 1957. Brazos River bar: a study of the significance of grain size parameters. Journal of Sedimentary Petrology 27, 3.-26.

Funder, S., Jennings, A.E., Kelly, M.J., 2004. Middle and late Quaternary glacial limits in Greenland, in: Ehlers, J.a.G., O.L. (Ed.), Quaternary Glaciations-Extent and Chronology, Part II. Elsevier, New York, pp. 425-430.

Geirsdottir, A., Andrews, J.T., Olafsdottir, S., Helgadottir, G., Hardardottir, J., 2002. A 36 ka record of iceberg rafting and sedimentation from north-west Iceland. Polar Research 21, 291-298.

Grobe, H., 1987. A Simple Method for the Determination of Ice-Rafted Debris in Sediment Cores. Polarforschung 57, 123-126.

Gudmundsdottir, E.R., Larsen, G., Eiriksson, J., 2012. Tephra stratigraphy on the North Icelandic shelf: extending tephrochronology into marine sediments off North Iceland. Boreas 41, 718-734.

Hagen, S., 1999a. North Atlantic paleoceanography and climate history during the last ~ 70 cal. ka years, Department of Geology. University of Tromso, Tromso, p. 110 pp.

Hagen, S., 1999b. North Atlantic Paleocedanography and climate history during the last ~70 cal. ka years, Department of Geology. University of Tromso, Tromso, Norway, p. 110.

Hagen, S., Hald, M., 2002. Variation in surface and deep water circulation in the Denmark Strait, North Atlantic, during marine isotope stages 3 and 2. Paleoceaography 17, 13-11 to 13-16 (10.1029/2001PA000632).

Hald, M., 1996. Greenland-Iceland margin cruise 1996. Universityof Tromso, , Tromso, Norway, p. 18.

Hardarson, B.S., Fitton, J.G., Hjartarson, A., 2008. Tertiary volcanism in Iceland. Jokull 58, 161-178.

Hass, C.H., 2002. A method to reduce the influebnce of ice-rafted debris on a grain size record from northern Fram Strait, Arctic Ocean. Polar Research 21, 299-306.

Hastings, A.D., 1960. Environment of Southeast Greenland. Quatermaster Research and Engineering Command.

Helgadottir, G., 1997. Paleoclimate (0 to >14 ka) of W. and NW Iceland: An Iceland/USA Contribution to P.A.L.E., Cruise Report B9-97. Marine Research Institute of Iceland, Reykjavik.

Hellmann, L., al., e., 2015. Timber logging in Central Siberia is the main source for recent Arctic driftwood. Arctic, Antarctic, and Alpine Research 47, 449-460.

Hemming, S.R., 2004. Heinrich Events: Massive late Pleistocene detritus layers of the North Atlantic and their global climate imprint. Reviews of Geophysics 42, RG1005/2004.

Henriksen, H., 2008. Geological history of Greenland. Geological Survey of Denmark and Greenland, Copenhagen.

Hesse, R., Khodabakhsh, S., 2016. Anatomy of Labrador Sea Heinrich layers. Marine Geology 380, 44-66.

Holland, D.M., Thomas, R.H., De Young, B., Ribergaard, M.H., Lyberth, B., 2008. Acceleration of Jakobshavn Isbrae triggered by warm subsurface ocean waters. Nature Geoscience 1, 659-664.

Hoppe, G., 1982. The Extent of the last Inland Ice Sheet of Iceland. Jökull 32, 3-11.

Hubbard, A., 2006. A multidisciplined approach to the reconstruction of Late Weischielian deglaciation of Iceland, in: Knight, P.G. (Ed.), Glacier Science and Environmental Change. Blackwell Publishing, Oxford, pp. 114-119.

Hörner, T., Stein, R., Fahl, K., Birgel, D., 2016. Post-glacial variability of sea ice cover, river run-off and biological production in the western Laptev Sea (Arctic Ocean) - A high resolution biomarker study. Quaternary Science Reviews 143, 133–149.

Huddard, A., Sugden, D., Dugmore, A., Norddahl, H., Petersson, H.G., 2006. A modelling insight into the Icelandic Last Glacial Maximum ice sheet. Quaternary Science Reviews 25, 2283-2296.

Hughes, T., 2011. A simple holistic hypothesis for the self-destruction of ice sheets. Quaternary Science Reviews 30, 1829-1845.

Jennings, A.E., Andrews, J.T., ÓCfoaigh, C., St. Onge, G., Sheldon, S., Belt, S.T., Cabedo-Sanz, P., Hillaire-Marcel, C., 2017. Ocean forcing of Ice Sheet Retreat in Central West Greenland from LGM through Deglaciation. Earth and Planetary Science Letters.

Jennings, A.E., Andrews, J.T., Wilson, L., 2011. Holocene environmental evolution of th SE Greenland Shelt north and south of the Denmark Strait: Irminger and East Greenland current interactions. Quaternary Science Reviews 30, 980-998.

Jennings, A.E., Gronvold, K., Hilberman, R., Smith, M., Hald, M., 2002. High resolution study of Icelandic tephras in the Kangerlussuaq Trough, southeast Greenland, during the last deglaciation. Journal of Quaternary Science 17, 747-757.

Jennings, A.E., Hald, M., Smith, L.M., Andrews, J.T., 2006. Freshwater forcing from the Greenland Ice Sheet during the Younger Dryas: Evidence from Southeastern Greenland shelf cores. Quaternary Science Reviews 25, 282-298.

Jennings, A.E., Helgadottir, 1994. Foraminiferal assemblages from the fjords and shelf of Eastern Greenland. Journal Foraminiferal Research 24, 123-144.

Jennings, A.E., Syvitski, J.P.M., Gerson, L., Gronvald, K., Geirsdottir, A., Hardardottir, J., Andrews, J.T., Hagen, S., 2000. Chronology and paleoenvironments during the late Weichselian deglaciation of the SW Iceland Shelf. Boreas 29, 167-183.

Jennings, A.E., Thordarson, T., Zalzal, K., Stoner, J.F., Hayward, C., Geirsdottir, A., Miller, G.H., 2014. Holocene tephra from Iceland and Alaska Record in SE Greenland Shelf sediments, in: Austin, W.E.N., Abbott, P.M., Davis, S., M., Pearce, N.J.G., Wastegard, S. (Eds.), Marine tephrachronology. Royal Society of London Special publication 398, pp. 157-193.

Jennings, A.E., Weiner, N.J., Helgadottir, G., Andrews, J.T., 2004a. Modern foraminiferal faunas of the Southwest to Northern Iceland shelf: Oceanographic and environmental controls. Journal of Foraminiferal Research 34, 180-207.

Jonkers, L., Prins, M.A., Moros, M., Weltje, G.J., Troelstra, S.R., Brummer, G.J.A., 2012. Temporal offsets between surface temperature, ice-rafting and bottom flow speed proxies in the glacial (MIS 3) northern North Atlantic. Quaternary Science Reviews 48, 43-53.

Khan, S.e.a., 2014. Sustained mass loss of the northeast Greenland ice sheet triggered by regional warming. Nat. Clim. Chang.4, 292-299. doi:10.1038/NCLIMATE2161 .

Knudsen, K.-L., Jiang, D., Jansen, E., Eiriksson, J., Heinemeier, J., Seidenkrantz, M.-S., 2003. Environmental changes off North Iceland during the deglaciation and the Holocene: foraminifera, diatoms and stable isotopes. Marine Micropaleontology 953, 1-33.

Knudsen, K.L., Jiang, H., Jansen, E., Eiriksson, J., Heinemeier, J., Seidenkrantz, M.S., 2004. Environmental changes off North Iceland during the deglaciation and the Holocene: foraminifera, diatoms and stable isotopes. Marine Micropaleontology 50, 273-305.

Kraus, W., 1958. Die hydrographischen Untersuchungen mit "Anton Dohrn" auf dem ost-westgronlandischen Schelf im September-Oktober 1955. Ber. Disch. Wiss. Komm. Meresforsch. 15, 77-104.

Kristjansdottir, G.B., Moros, M., Andrews, J.T., Jennings, A.E., 2016 Holocene Mg/Ca, alkenones, and light stable isotope measurements on the outer North Iceland shelf (MD99-2269): A comparison of proxy data The Holocene, 1-11.

Kuijpers, A., Troelstra, S.R., Prins, M.A., Linthout, K., Akhmetzhanov, A., Bouryak, S., Bachmann, M.F., Lassen, S., Rasmussen, S., Jensen, J.B., 2003. Late Quaternary sedimentary processes and ocean circulation changes at the Southeast Greenland margin. Marine Geology 195, 109-129.

Labeyrie, L., Jansen, E., Cortijo, E., 2003. Les rapports de campagnes a la mer MD114/IMAGES V. Institut Polaire Francais Paul-Emile Victor, Brest.

Lambeck, K., Rouby, H., Purcell, A., Sun, Y., Sambridge, M., 2014. Sea level and global ice volumes from the Last Glacial Maximum to the Holocene. Proceedings of the National Academy of Sciences of the United States of America 111, 15296-15303.

Larsen, B., 1983. Geology of the Greenland-Iceland Ridge in the Denmark Strait, in: Bott, M.H.P., Saxov, S., Talwani, M., Thiede, J. (Eds.), Structure and Development of the Greenland-Scotland Ridge. Plenum Publishing Corp., London, pp. 425-444.

Larsen, M., Hamberg, L., Olaussen, S., Norgaard-Pedersen, N., Stemmerik, L., 1999. Basin evolution in Southern East Greenland: An outcrop analog for Cretaceous-Paleogene basins on the North Alantic volcanic margins. AAPG Bulletin 83, 1236-1261.

Lecavalier, B.S., Milne, G.A., Simpson, M.J.R., Wake, L., Huybrechts, P., Tarasov, L., Kjeldsen, K.K., Funder, S., Long, A.J., Woodroffe, S., Dyke, A.S., Larsen, N.K., 2014. A model of Greenland ice sheet deglaciation constrained by observations of relative sea level and ice extent. Quaternary Science Reviews 102, 54-84.

Lind, E.W., Lilja, C., Wastegard, S., Pearce, N.J.G., 2016. Revisiting the Borrobol Tephra. Boreas.

Lohne, O.S., Mangerud, J., Birks, H.H., 2013. Precise C-14 ages of the Vedde and Saksunarvatn ashes and the Younger Dryas boundaries from western Norway and their comparison with the Greenland Ice Core (GICC05) chronology. Journal of Quaternary Science 28, 490-500.

Marcott, S.A., Bauska, T.K., Buizert, C., Steig, E.J., Rosen, J.L., Cuffey, K.M., Fudge, T.J., Severinghaus, J.P., Ahn, J., Kalk, M.L., McConnell, J.R., Sowers, T., Taylor, K.C., White, J.W.C., Brook, E.J., 2014. Centennial-scale changes in the global carbon cycle during the last deglaciation. Nature 514, 616-+.

Manley, W.F., Jennings, A.E., 1996. Radiocarbon Date List VIII: Eastern Canadian Arctic, Labrador, Northern Quebec, East Greenland Shelf, Iceland Shelf, and Antarctica. INSTAAR, University of Colorado, p. 163 pp.

Massé, G., Belt, S.T., Crosta, X., Schmidt, S., Snape, I., Thomas, D.N. and Rowland, S.J. (2011) Highly branched isoprenoids as proxies for variable sea ice conditions in the Southern Ocean. *Antarctic Science* 23, 487-498

Mienert, J., 1990. Forschungsschiff POSEIDON. Reise Nr. 175/1 9/10-21/10 1990. GEOMAR, Kiel.

Mienert, J., Andrews, J.T., Milliman, J.D., 1992. The East Greenland Continental Margin (65 N) since the last deglaciation: Changes in sea floor properties and ocean circulation. Marine Geology 106, 217-238.

Minansy, B., 2010. Fuzzy k means extragrades, performance measures & fuzzy linear discriminant analysis. The University of Sydney, Australia, p. 28 pp.

Minasny, B., McBratney, A.B., 2002. FuzMe version 3.0. Australian Center for Precision Agriculture, Universityof Sydney, Australia.

.Moros, M., Andrews, J.T., Eberl, D.D., Jansen, E., 2006. The Holocene history of drift ice in the northern North Atlantic: Evidence for different spatial and temporal modes. Palaeoceanography 21, 1 of 10. doi:10.1029/2005PA001214.

Mortensen, A.K., Biglier, M., Gronvold, K., Steffensen, J.P., Johnsen, S.J., 2005. Volcanic ash layers from the last Glacial Termination in the NGRIP ice core. Journal of Quaternary Science 20, 209-220

Müller, J., Stein, R., 2014. High-resolution record of late glacial sea ice changes in Fram Strait corroborates ice-ocean interactions during abrupt climate shifts. Earth and Planetary Science Letters 403, 446–455.

Norddahl, H., 1990. Late Weiechelian and early Holocene deglaciation history of Iceland. Jökull 40, 27-50.

Norðdahl, H., Ingolfsson, O., 2015. Collapse of the Icelandic ice sheet controlled by sea-level rise? Arktos, pp 1-18.

O Cofaigh, C., Dowdeswell, J.A., Evans, J., Kenyon, N.H., Taylor, J., Mienert, A., Wilken, M., 2004. Timing and significance of glacially influenced mass-wasting in the submarine channels of the Greenland Basin. Marine Geology 207, 39-54.

Ogilvie, A.E.J., 1992. Documentary evidence for changes in the climate of Iceland, A.D. 1500 to 1800, in: Bradley, R.S., Jones, P.D. (Eds.), Climate since A.D. 1500. Routledge, London, pp. 92-117.

Ogilvie, A.E.J., Jonsdottir, I., 2000. Sea ice, climate, amd Icelandic fisheries in the eighteenth and nineteenth centuries. Arctic 53, 383-394.

Olafsdottir, S., 2004. Currents and climate on the northwest shelf of Iceland during the deglaciation: high-resolution foraminiferal research, Department of Geosciences. University of Iceland, Reykjavik, p. 117.

Olafsdottir, S., Jennings, A.E., Geirsdottir, A., Andrews, J., Miller, G.H., 2010. Holocene variability of the North Atlantic Irminger current on the south- and northwest shelf of Iceland. Marine Micropaleontology 77, 101-118.

Patton, H., Hubbard, A., Bradwell, T., Schomacker, A., 2017. The configuration, sensitivity and rapid retreat of the Late Weischelian Icelandic Ice Sheet. Earth-Science Reviews 166, 223-245.

Petursson, H.G., Norddahl, H., Ingolfsson, O., 2015. Late Weichselian history of relative sea level changes in iceland during a collapse and subsequent retreat of marine based ice sheet. Cuadernos De Investigacion Geografica 41, 261-277.

Peltier, W.R., Argus, D.F., Drummond, R., 2015. Space geodesy constrains ice age terminal deglaciation: The global ICE-6G_C (VM5a) model. Journal of Geophysical Research-Solid Earth 120, 450-487.

Perner, K., Jennings, A.E., Moros, M., Andrews, J.T., Wacker, L., 2016. Millennial scale mid to late Holocene oscillation of the East Greenland and Irminger Current on the south-eastern Greenland shelf Journal of Quaternary Science.

Praetorius, S.K., Mix, A.C., 2014. Synchronization of North Pacific and Greenland climates preceded abrupt deglacial warming. Science 345, 444-448.

Praetorious, S.K., Mix, A.C., 2016. Did synchronized ocean warming in the North Pacific and North Atlantic trigger a deglacial tipping point in the Northern Hemiepshere? Past Global Change 24, 10-11.

Principato, S.M., 2003. The late Quaternary history of eastern Vestfirdir, NW Iceland, Geological Sciences. University of Colorado, Boulder, p. 258.

Principato, S.M., Geirsdottir, A., Johannsdottir, G.E., Andrews, J.T., 2006. Late Quaternary glacial and deglacial history of eastern Vestfirdir, Iceland using cosmogenic isotope (36Cl) exposure ages and marine cores. Journal of Quaternary Science 21, 271-286.

Principato, S.M., Moyer, A.N., Hampsch, A.G., Ipsen, H.A., 2016. Using GIS and streamlined landforms to interpret palaeo-ice flow in northern Iceland. Boreas 45, 470-482.

Prins, M.A., Bouwer, L.M., Beets, C.J., Troelstra, S.R., Weltje, G.J., Kruk, R.W., Kruijpers, A., Vroon, P.Z., 2002. Ocean circulation and iceberg discharge in the glacial North Atlantic: Inferences from unmixing of sediment sizes. Geology 30, 555-558.

Quillmann, U., 2006. Holocene environmental variability in Isafjardardjup and its tributary fjords, NW Iceland, Geological Sciences. University of Colorado, Boulder, p. 280.

Quillmann, U., Andrews, J.T., Jennings, A.E., 2009. Radiocarbon Date List XI: East Greenland shelf, West Greenland Shelf, Labrador Sea. Baffin Island shelf, Baffin Bay, Nares Strait, and Southwest to Northwest Icelandic shelf. Occasional Paper No. 59, INSTAAR, University of Colorado, Boulder, Boulder, p. 68.

Quillmann, U., Jennings, A.E., Andrews, J.T., 2010. Reconstructing Holocene paleocliumate and paleoceanography in Isafjaradrdjup, Northwest Iceland, from two fjord cores overprinted by relative sea level and local hydrographic changes. Journal of Quaternary Science 25, 1144-1159.

Rasmussen, S.O., Bigler, M., Blockley, S.P., Blunier, T., Buchardt, S.L., Clausen, H.B., Cvijanovic, I., Dahl-Jensen, D., Johnsen, S.J., Fischer, H., Gkinis, V., Guillevic, M., Hoek, W.Z., Lowe, J.J., Pedro, J.B., Popp, T., Seierstad, I.K., Steffensen, J.P., Svensson, A.M., Vallelonga, P., Vinther, B.M., Walker, M.J.C., Wheatley, J.J., Winstrup, M., 2014. A stratigraphic framework for abrupt climatic changes during the Last Glacial period based on three synchronized Greenland ice-core records: refining and extending the INTIMATE event stratigraphy. Quaternary Science Reviews 106, 14-28.

Roy, K., Peltier, W.R., 2015. Glacial isostatic adjustment, relative sea level history and mantle viscosity: reconciling relative sea level model predictions for the US East coast with geological constraints. Geophysical Journal International 201, 1156-1181.

Rytter, F., Knudsen, K.-L., Seidenkrantz, M.-S., Eiriksson, J., 2002. Modern distribution on benthic foraminifera on the North Icelandic shelf and slope. Journal of Foraminferal Research 32, 217-244.

Sarna-Wojcicki, A.M., Bowman, H.R., Meyer, C.E., Russell, P.C., Woodward, M.J., G., M., Rowe, J.J.J., Baedecker, P.A., Asaro, F., Michael, H., 1984. Chemical analyses, correlations, and ages of Upper Pliocene and Pleistocene as layers of East-Central and southern California. United States Geological Survey, Washington, DC, p. 33 pp.

Sarnthein, M., Balmer, S., Grootes, P.M., Mudelsee, M., 2015. Planktic and benthic c-14 reservoir ages for three ocean basins, calibrated by a suite of c-14 plateaus in the glacial-to-deglacial atmospheric c-14 record. Radiocarbon 57, 129-151.

Seale, A., Christoffersen, P., Mugford, R.I., O'Leary, M., 2011. Ocean forcing of the Greenland Ice Sheet: Calving fronts and patterns of retreat identified by automatic satellite monitoring of eastern outlet glaciers. Journal of Geophysical Research-Earth Surface 116, 1 of 16.

Seidov, D., Baranova, O.K., Boyer, T., Cross, S., Mishonov, A., Parsons, A.R., 2016. Northwest Atlantic regional ocean climatology. NOAA Atlas NESDIS80, in: A.V.Mishonov (Ed.), 56pp.

Sinclair, G., Carlson, A.E., Mix, A.C., Lecavalier, B.S., Milne, G., Mathias, A., Buizert, C., DeConto, R., 2016. Diachronous retreat of the Greenland ice sheet during the last deglaciation. Quaternary Science Reviews 145, 243-258.

Smith, L.M., Andrews, J.T., Castaneda, I.S., Kristjansdottir, G.B., Jennings, A.E., Sveinbjjronsdottir, A.E., 2005. Temperature reconstructions for SW amd N Iceland

waters over the last 10,000 cal yr B.P. based on d18O records from planktic and benthic Foraminifera. Quaternary Science Reviews 24, 1723-1740.

Smith, L.M., Licht, K.J., 2000. Radiocarbon Date List IX: Antarctica, Arctic Ocean, and the Northern North Atlantic. INSTAAR Occasional paper No. 54, University of Colorado, 138 pp, Boulder, CO, p. 138.

Stein, A.B., 1996. Seismic stratigraphy and seafloor morphology of the Langerlussuaq region, East Greenland: Evidence for glaciations to the Continental Shelf break during the late Weischelian Age and earlier, Geological Sciences. University of Colorado, Boulder, p. 293 pp.

Stein, R., Fahl, K., Schade, I., Manerung, A., Wassmuth, S., Niessen, F., Nam, S., 2017. Holocene variability in sea ice cover, primary production, and Pacific-Water inflow and climate change in the Chukchi and East Siberian Seas (Arctic Ocean). Journal of Quaternary Science 32, 362–379.

Stern, J.V., Lisiecki, L.E., 2013. North Atlantic circulation and reservoir age changes over the past 41,000years. Geophysical Research Letters 40, 3693-3697.

Syvitski, J.P., Jennings, A.E., Andrews, J.T., 1999. High-Resolution Seismic Evidence for Multiple Glaciation across the Southwest Iceland Shelf. Arctic and Alpine Research 31, 50-57.

Syvitski, J.P.M., Andrews, J.T., Dowdeswell, J.A., 1996. Sediment deposition in an iceberg-dominated Glacimarine Environment, East Greenland: Basin Fill Implications. Global and Planetary Change 12, 251-270.

Syvitski, J.P.M., Stein, A., Andrews, J.T., Milliman, J.D., 2001. Icebergs and seafloor of the East Greenland (Kangerlussuaq) continental margin. Arctic, Antarctic and Alpine Research 33, 52-61.

Tanner, W.F., 1965. Cause and Development of an Ice Age. The Journal of Geology 73.

Thiagarajan, N., Subhas, A.V., Southon, J.R., Eiler, J.M., Adkins, J.F., 2014. Abrupt pre-Bolling-Allerod warming and circulation changes in the deep ocean. Nature 511, 75-U409.

Tarasov, L., Peltier, W.R., 2002. Greenland glacial history and local geodynamic consequences. Geophysical Journal International 150, 198-229.

Thordardottir, T., 1984. Primary Production North of Iceland in relation to Water Masses in May-June 1970-1980. Conference for the Exploration of the Sea, C.M. 1984/L20, 1-17.

Thordardottir, T., 1986. Timing and Duration of Spring Blooming South and Southwest of Iceland. NATO ASI Series G-7, 345-360.

Thornalley, D.J.R., Barker, S., Broecker, W.S., Elderfield, H., McCave, I.N., 2011. The Deglacial Evolution of North Atlantic Deep Convection. Science 331, 202-205.

Thornalley, D.J.R., Bauch, H.A., Gebbie, G., Guo, W., Ziegler, M., Bernasconi, S.M., Barker, S., Skinner, L.C., Yu, J., 2015. A warm and poorly ventilated deep Arctic Mediterranean during the last glacial period. Science 349, 706-710.

Thors, K., 1974. Sediments of the Vestfirdir Shelf, NW Iceland. Univ. of Manchester.

Turney, C.S.M., Fogwill, C.J., Lenton, T.M., Jones, R.T., 2016. Tipping Points: Lessons from the Past for the Future. Past Global Change 24, 3.

van Kreveld, S., Sarthein, M., Erlenkeuser, H., Grootes, P., Jung, S., Nadeau, M.J., Pflaumann, U., Voelker, A., 2000. Potential links between surging ice sheets, circulation changes, and the Dansgaard-Oeschger cycles in the Irminger Sea, 60-18 ka. Paleoceanography 15, 425-442.

Vasskog, K., Langebroek, P.M., Andrews, J.T., Nilsen, J.E.O., Nesje, A., 2015. The Greenland Ice Sheet during the last glacial cycle: Current ice loss and contribution to sea-level rise from a palaeoclimatic perspective. Earth-Science Reviews 150, 45-67.

Vinther, B.M., Clausen, H.B., Fisher, D.A., Koerner, R.M., Johnsen, S.J., Andersen, K.K., Dahl-Jensen, D., Rasmussen, S.O., Steffensen, J.P., Svensson, A.M., 2008. Synchronizing ice cores from the Renland and Agassiz ice caps to the Greenland ice core chronology. Journal of Geophysical Research-Atmospheres 113. 1 of 10. 10.1029/2007JD009143.

Voelker, A.H.L., Haflidason, H., 2015. Refining the Icelandic tephrachronology of the last glacial period - The deep-sea core P52644 record from the southern Greenland Sea. Global and Planetary Change 131, 35-62.

Weltje, G.J., Prins, M.A., 2003. Muddled or mixed? Inferring palaeoclimate from size distributions of deep-sea clastics. Sedimentary Geology 162, 39-62.

Weltje, G.J., Prins, M.A., 2007. Genetically meaningful decomposition of grain-size distributions. Sedimentary Geology 202, 409-424.

Xiao, X., Zhao, M., Knudsen, K.L., Sha, L., Eiríksson, J., Gudmundsdóttir, E., Jiang, H., Guo, Z., 2017. Deglacial and Holocene sea-ice variability northof Iceland and response to ocean circulation changes. Earth and Planetary Science Letters 472, 14-24.

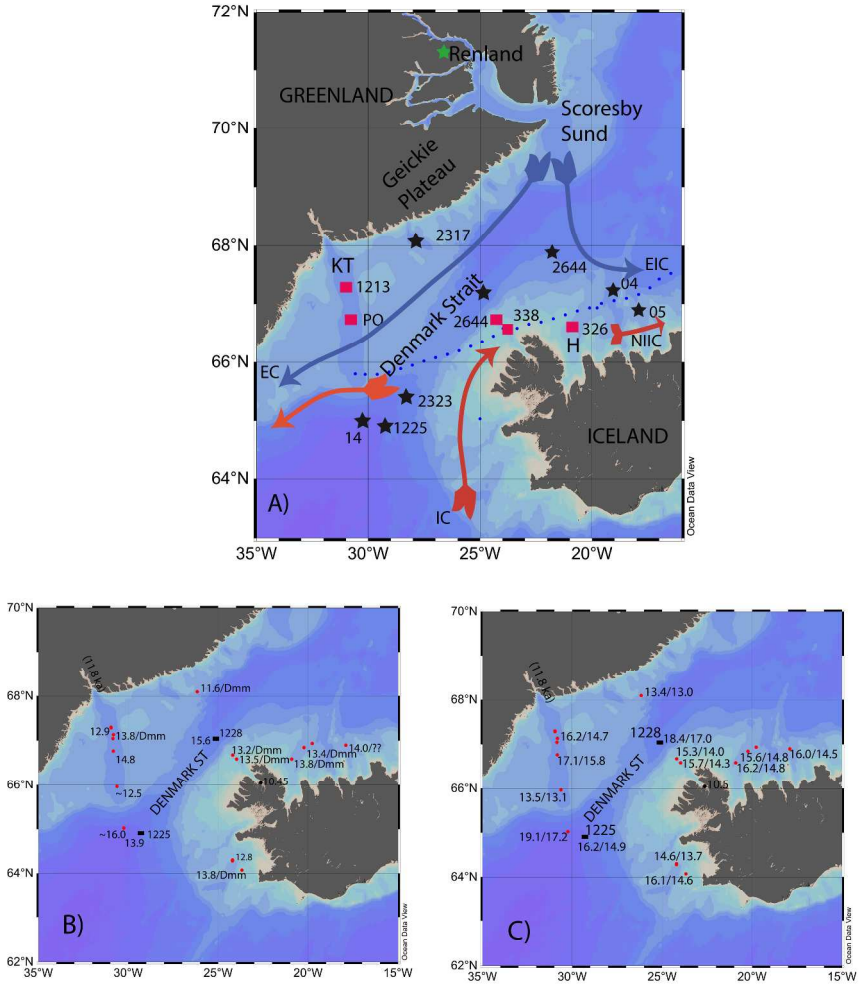

Figure 1A: Map of the Denmark Strait area showing the primary cores (solid squares), cores noted in the text and providing information (filled stars; Suppl.Table 1). Dotted blue line = average position of the sea ice edge (15% coverage) April AD 1870-1920 (Divine and Dick, 2006). KT = Kangerlussuaq Trough, H = Húnaflói, the Djúpáll Trough is located at core MD99-2264. Surface Atlantic Currents: Irminger Current = IC, North Iceland Irminger Current (NIIC); cold surface Arctic/Polar Currents: East Greenland Current = EC, East Iceland Current = EIC. B) Map of basal uncorrected 14C dates and whether the core penetrated a basal diamicton (Dmm). Black squares show the two cores with stable isotope records across the glacial/deglacial transition. C) The calibrated 14C dates with values based on a ΔR of 0 versus the sliding scale ΔR estimates (Table 2). The number in brackets along Kangerlussuaq Fjord (11.8 cal ka BP) is the average cosmogenic date (Dyke et al., 2014).

279x361mm (300 x 300 DPI)

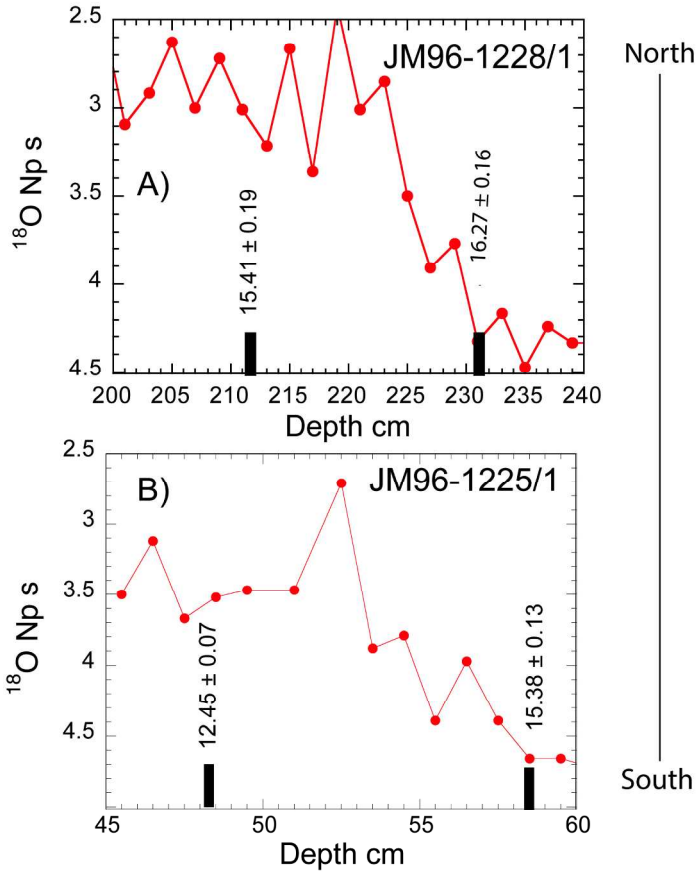

Figure 2: Neogloboquadrina pachyderma s δ18O records from north and south of Denmark Strait (Hagen, 1999) illustrating the transition from glacial to interstadial values, and the differences in the radiocarbon dates that we assume is associated with regional variations in the ocean reservoir correction (see text).

258x329mm (300 x 300 DPI)

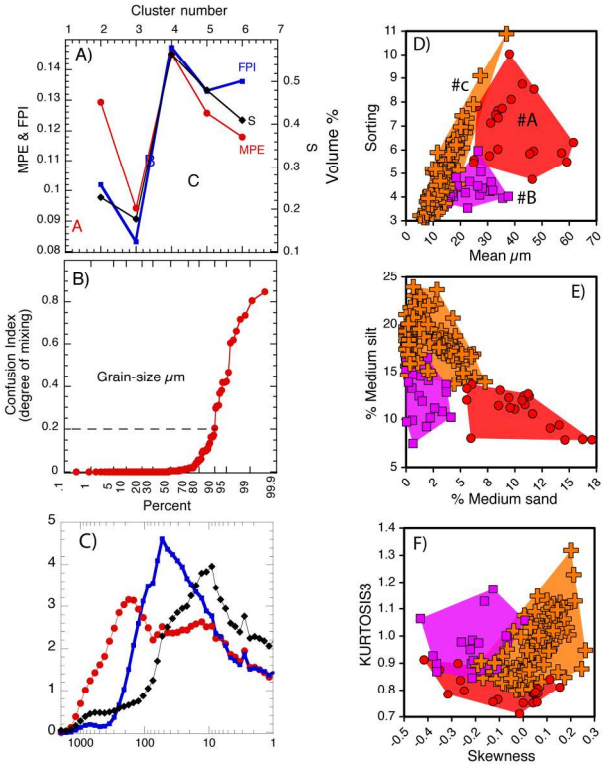

Figure 3: Analysis of the grain-size spectra (n = 191). A) Plot of the 3 performance indictors in FuzMe (Minansy, 2010; Minasny and McBratney, 2002) (MPE= modified partition entropy, FPI = fuzziness performance indicator, S = Compactness and separation validity function) indicating the optimal solution of 4 Grain-size mode (GSM) clusters; B) Probability plot of the Confusion Index (CI) (0 = certainty of cluster membership, 1 = equal mixture of the 3 grain-size modes C) Plot of the average grain-size spectra for the 3 GSMs; D) Plot of the mean grain-size (μm) and sorting; E) Plot of the percentages of medium sand versus medium silt; and F) Plot of aspects of the shape of the grain-size spectra, Skewness versus Kurtosis (Folk and Ward, 1957; Blott and Pye, 2001).

226x214mm (300 x 300 DPI)

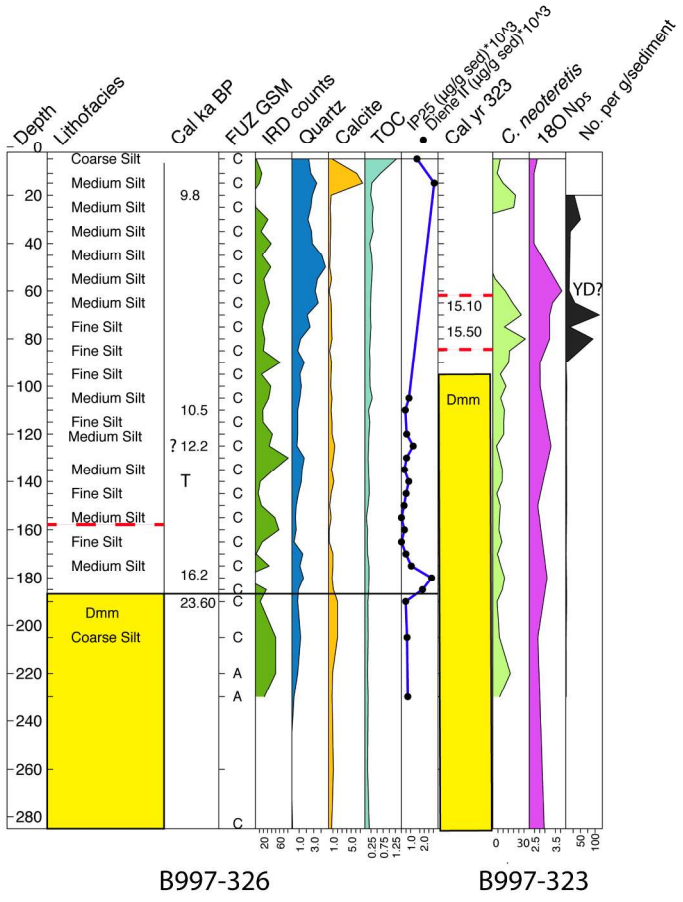

Fig. 4

269x352mm (300 x 300 DPI)

A

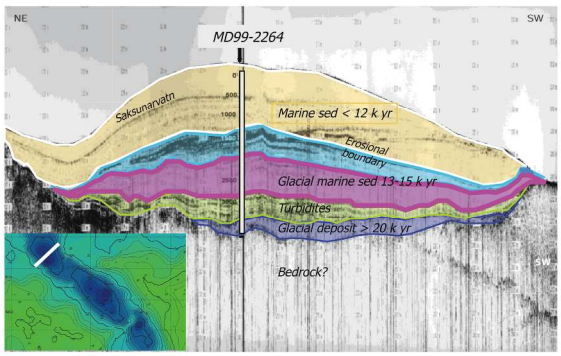

B

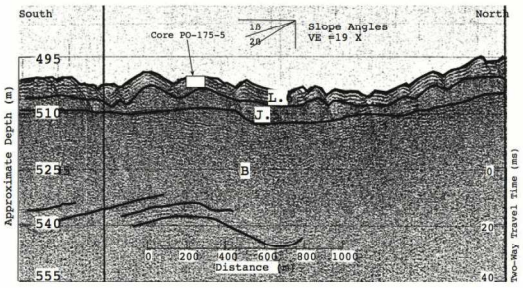

C

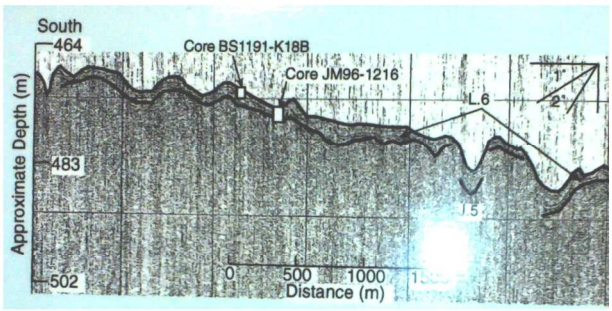

Fig. 5

279x361mm (300 x 300 DPI)

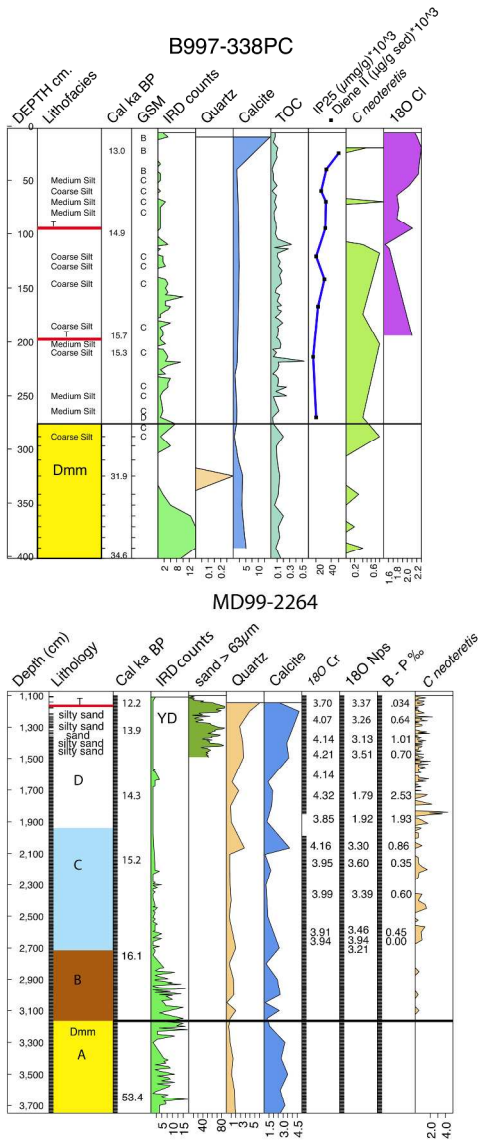

Fig. 6

279x361mm (300 x 300 DPI)

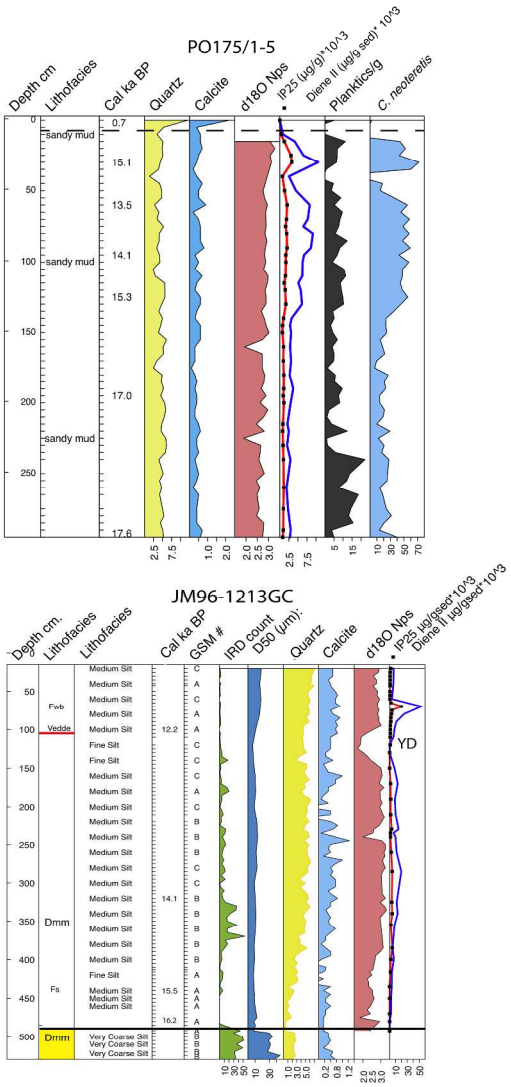

Fig. 7

279x361mm (300 x 300 DPI)

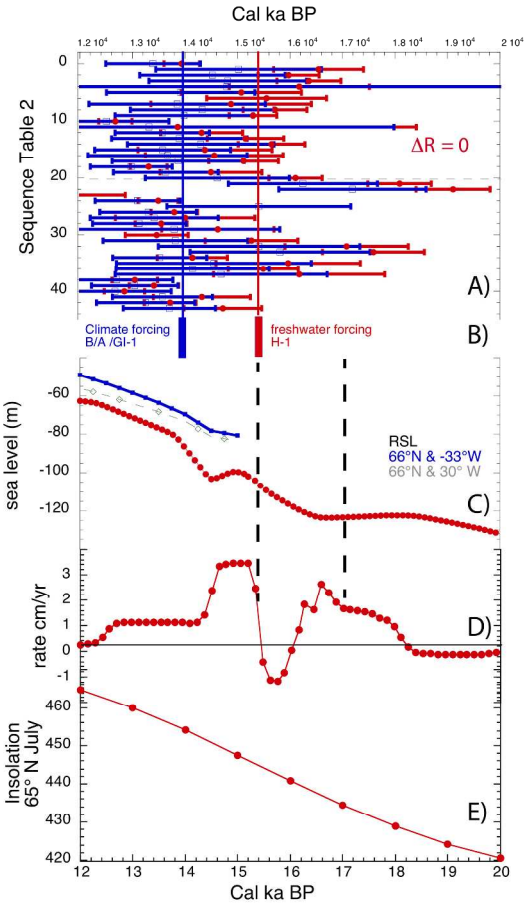

Figure 8: Global and regional parameters operating in the period between 12 and 17 cal ka BP. A) Plot of median calibrated ages and the 95% confidence interval for sites discussed in this paper (Fig. 1, see Table 2) using ΔR = 0 (red) and ΔR ≤ 1000 yr (blue). The vertical solid blue and red lines represent the median ages for the basal dates for the two ΔR options; C) Eustatic sea level (Lambeck et al., 2014) and estimates of relative sea level change (RSL) at specific latitudes and longitudes (Peltier, person. commun. 2016). D) Rate of change of global sea level (C); and E) July Insolation at 65°N (Berger and Loutre, 1991);

279x361mm (300 x 300 DPI)

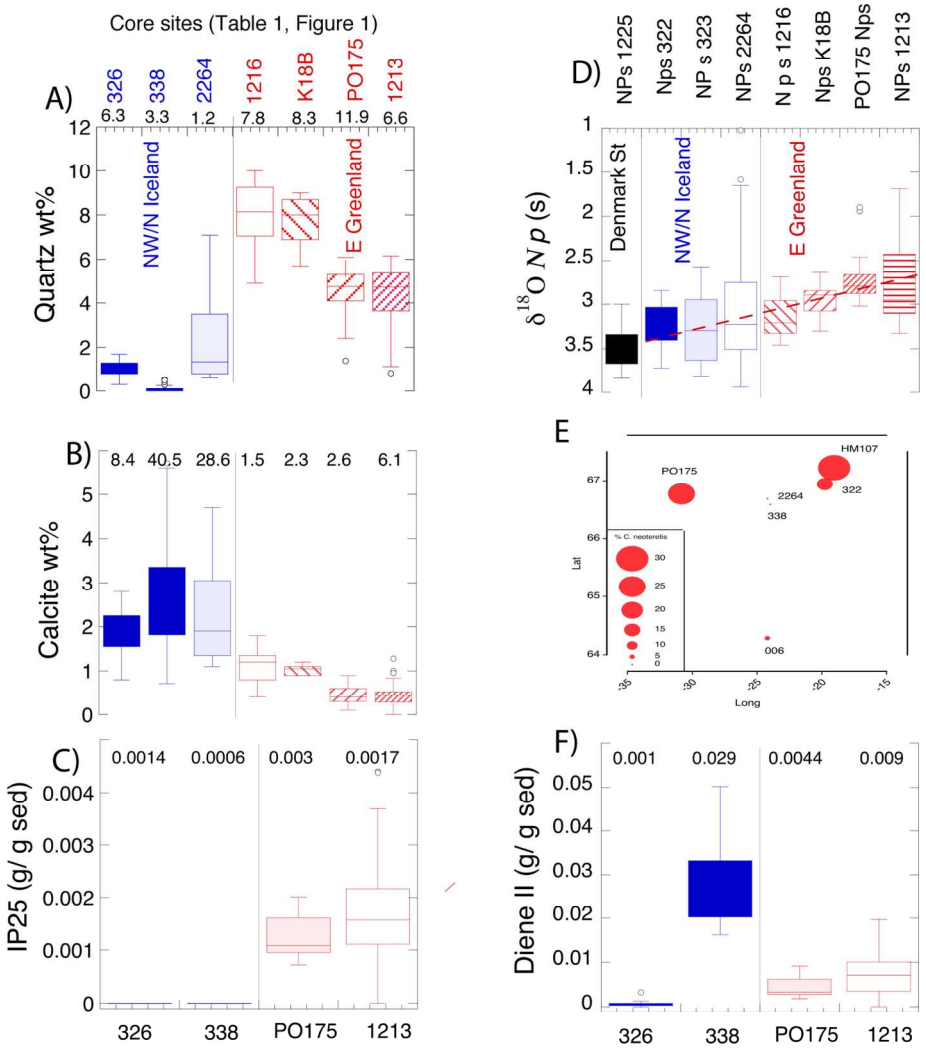

Figure 9: Box plots of surface & near-surface environment proxies across Denmark Strait (east to west) between 12 to ~15 cal ka BP--- –numbers give the wt% of modern samples showing: A) Weight % quartz; B) Weight % calcite; and C) IP25; D) δ18O for the near-surface polar planktonic foraminifera Neogloboquadrina pachyderma; E) Map of the % of C. neoteretis for the deglacial interval > 12 cal ka BP; F) Diene II.

178x207mm (300 x 300 DPI)

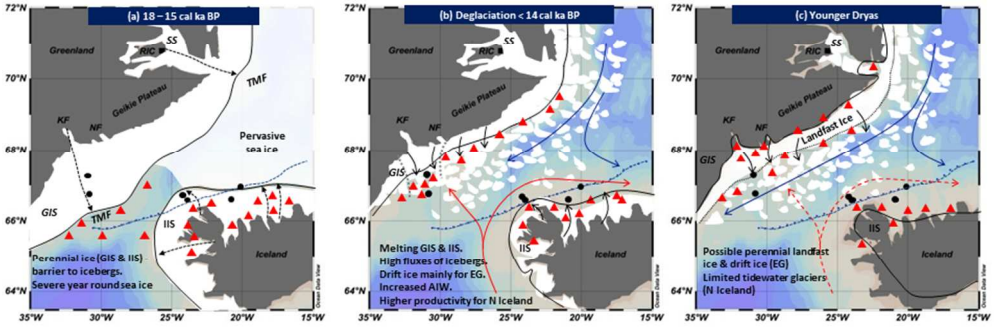

Figure 10: Simplified scenarios of conditions in Denmark Strait at the end of MIS2 and during the initial period of deglaciation. Red triangles represent icebergs and the white patches represent sea ice. Black dots refer to the core locations as listed in Table 1. Red arrows represent warm surface (Atlantic Water) currents and the dark blue represents the export of cold Polar Water. A) Ice Sheet extent during the LGM; B) conditions during deglaciation, and C) Conditions at the YD interval.

254x190mm (96 x 96 DPI)

Supplemental Material

Methods

Coarse ice-rafted sediment >2 mm: The number of clasts > 2 mm were counted in 2-cm vertical increments on X-radiographs of the split cores (Andrews et al., 1997; Geirsdottir et al., 2002). These counts are used as the most definitive evidence of ice-rafting debris (IRD) associated with deposition from icebergs (Andrews, 2000)(Andrews, 2000).

Grain-size: Lithofacies were based on visual inspection and examination of X-radiographs on split cores. Grain-size data were obtained on 162 samples from cores B997-322, -323, -326, -328 and JM96-1213 with boundaries between 2000 and 2 µm. The samples were processed on the Malvern long-bed laser system after treatment with hydrogen peroxide to remove any organics. Samples were not decalcified as detrital carbonate can be an important signal of the export of sediment from or from the extensive limestone outcrops in N Greenland and the Canadian Arctic Archipelago. Furthermore, decalcification of samples from MD99-2269 (Andrews et all, 2003) resulted in little change in grain-size properties. Grain-size statistics were obtained using Gradistat (Blott and Pye, 2001)(Blott and Pye, 2001). Rather than just report variations in parameters, such as mean grain-size, we sought to more rigorously characterize the grain-size distributions (Weltje and Prins, 2003; Weltje and Prins, 2007).(Weltje and Prins, 2003; Weltje and Prins, 2007)

X-ray diffraction of < 2 mm sediment fraction: Quantitative X-ray diffraction (qXRD) analysis of the < 2 mm sediment fraction was undertaken using the method outlined by Eberl (Eberl, 2003)(Eberl, 2003) is which 10% by weight of ZnO is added to the sample, milled for 5 minutes in a McCrone mill, dried, and then loaded into a Siemens D5000 X-ray diffractometer. Each sample runs for 100 minutes with scanning taking place in 0.02 2-theta steps between 5 and 65° 2-theta, and measured intensities recorded every 2 secs. The data are then downloaded and weight% of minerals estimated using the Excel macro program Rockjock v6 (Eberl, 2003). qXRD data from the area have been reported previously (Andrews, 2008; Andrews and Eberl, 2007). The QXRD data have been used in a sediment umixing model (Andrews and Eberl, 2012) to better understand the varying contributions from possible bedrock source areas (Andrews et al., 2015).

Light Stable Isotopes: $\delta^{18}O$ and $\delta^{13}C$ data have been obtained on both benthic and planktonic foraminifera for our sites, but at varying levels of resolution. Details on the processing of the samples are given in Olafsdottir (Olafsdottir, 2004). Data were obtained on the dominant polar planktonic foraminifera *Neogloboquadrina pachyderma* s and on several species of benthic foraminifera. We compare our data with $\delta^{18}O$ values o *Neogloboquadrina pachyderma* s from cores in the area of Denmark Strait, namely JM96-1225, -1228 (Hagen, 1999b; Hagen and Hald, 2002) and MD99-2323 (Dunhill, 2005) (Fig. 1). There is also a considerable body of information on both modern (surface) and Holocene $\delta^{18}O$ ratios on both planktonic and benthic foraminifera from both shelves (Castaneda et al., 2004; Jennings et al., 2011; Knudsen et al., 2004; Kristjansdottir et al., 2016 ; Smith et al., 2005).

Foraminifera assemblages: Details of the sample processing for foraminifera are given in Olafsdottir (Olafsdottir, 2004) and Jennings et al (Jennings et al., 2004). Interpretations are based on the analysis of the occurrence of species in seafloor sediments collected in the 1990s (Jennings and Helgadottir, 1994; Jennings et al., 2004; Rytter et al., 2002).

Biomarkers: Biomarker analyses (IP_{25} and $C_{25:2}$) were performed on 107 samples from cores B997-326 (n = 21), -338 (n = 8), JM96-1213 (n = 43) and 175PO/1-5 (n = 35), using methods described previously (Belt et al., 2012; Belt et al., 2013). Briefly, two internal standards, 7-hexylnonadecane and 9-octylheptadec-8-ene (each 0.10 µg) were added to freeze-dried sediment samples (ca. 3 g) to permit quantification of IP_{25} and $C_{25:2}$. Samples were then extracted using dichloromethane/methanol (3 x 3 mL; 2:1 v/v; ultrasonication; 15 min). Dried total organic extracts were then partially purified using column chromatography (silica; hexane; 6 mL) and further fractionated into saturated and unsaturated components using silver ion solid-phase extraction (SPE) material (100 mg; Supelco discovery® Ag-Ion). Saturated and unsaturated (including IP_{25} and $C_{25:2}$) hydrocarbons were with hexane (1 mL) and acetone (2 mL), respectively. Analysis of purified fractions was carried out using gas chromatography–mass spectrometry (GC–MS) as described previously (Belt et al., 2012). Mass spectrometric analysis was mainly carried out in single-ion monitoring (SIM) mode. IP_{25} and $C_{25:2}$ were identified on the basis of their characteristic GC retention indices and mass spectra obtained from standards, while quantification was achieved by comparison of mass spectral responses of selected ions (IP_{25}: *m/z* 350; $C_{25:2}$: *m/z* 348) with that of the internal standard (*m/z* 350) and normalized according to relative response factors and sediment masses (Belt et al.,

2012). Analytical reproducibility was monitored using standard sediment with a known concentration of IP_{25} (8 %, n = 8).

Depth/age radiocarbon models:

In sites MD99-2264 and JM96-1213 there are sufficient dates over a reasonable depth span to construct depth/age curves using the two ΔR options (Suppl. Table 1). We used the flexible Bayesian program (Bacon) (Blaauw and Christen, 2011) to reconstruct depth/age plots (Suppl. Fig. 1)--- in Figures 6B and 7B these are simplified and only the median ages are plotted. Accumulation rates were high at both sites and both models tended to overestimate the age of sediment at the depth of the Vedde tephra (Suppl. Fig. 1) indicating either a change in the prior or a need to change ΔR. In both cores the rates of accumulation are essentially constant. The variations of age versus depth in PO175/1-5 (Suppl. Table 1) were such that we have not used an age model in Fig. 7A but the results of the two alternative ΔRs are plotted on Suppl. Fig. 1.

Caption Suppl. Fig. 1: Outputs from the Bayesian calibration program "Bacon" (Blaauw and Christen, 2011, 2016) for MD99-2264, JM96-1213, and PO175/105 showing the results with the two different ocean reservoir corrections (see text). The single "best" model is the faint red dashed line. Grey stippled areas are the 95% confidence limits

Suppl. Table 1:

This table lists all the radiocarbon dates used in this paper and shows the number of the date listed on Fig. 8 (col A), material dated (B), original data and error (E & F). Cols G to K give the calibrated 95% age range, median and sigma error with a ΔR = 0, and cols L to R give the estimated ΔR, error, 95% age range, median date and error for calibrations with the variable deltaR (see text).

Suppl. Table 2:

Geochemical analyses for tephras noted in this paper. Data from the University of Colorado's microprobe analysis of the Lipari obsidian standard (Hunt and Hill, 1996)is listed first followed by the tephras in B997-338 and -323 and -326 (Andrews and Helgadottir, 2003; Andrews et al., 2013).

References cited

Andrews, J.T., 2000. Icebergs and Iceberg Rafted Detritus (IRD) in the North Atlantic: Facts and Assumptions. Oceanography 13, 100-108.

Andrews, J.T., 2008. The role of the Iceland Ice Sheet in sediment delivery to the North Atlantic during the late Quaternary: how important was it? Evidence from the area of Denmark Strait. Journal of Quaternary Science 23`, 3-20.

Andrews, J.T., Bjork, A.A., Eberl, D.D., Jennings, A.E., Verplanck, E.P., 2015. Significant differences in late Quaternary bedrock erosion and transportation: East versus West Greenland ~ 70°N and the evolution of glacial landscapes. Journal of Quaternary Science 30, 452-463.

Andrews, J.T., Eberl, D.D., 2007. Quantitative mineralogy of surface sediments on the Iceland shelf, and application to down-core studies of Holocene ice-rafted sediments. Journal of Sedimentary Research 77, 469-479.

Andrews, J.T., Eberl, D.D., 2012. Determination of sediment provenance by unmixing the mineralogy of source-area sediments: The "SedUnMix" program. Marine Geology 291, 24-33.

Andrews, J.T., Helgadottir, G., 2003. Late Quaternary ice cap extent and deglaciation of Hunafloaall, NorthWest Iceland: Evidence from marine cores. Arctic, Antarctic, and Alpine Research 35, 218-232.

Andrews, J.T., Kristjansdottir, G.B., Eberl, D.D., Jennings, A.E., 2013. A quantitative X-ray diffraction inventory of tephra and volcanic glass inputs into the Holocene marine sediment archives of Iceland: A contribution to V.A.S.T. Polar Research, 1-15.

Andrews, J.T., Smith, L.M., Preston, R., Cooper, T., Jennings, A.E., 1997. Spatial and temporal patterns of iceberg rafting (IRD) along the East Greenland margin, ca. 68 N, over the last 14 cal.ka. Journal of Quaternary Science 12, 1-13.

Belt, S.T., Brown, T.A., Navarro Rodriguez, A., Cabedo Sanz, P., Tonkin, A., Ingle, R., 2012. A reproducible method for the extraction, identification and quantification of the Arctic sea ice proxy IP25 from marine sediments. Analytical Methods 4, 705-713.

Belt, S.T., Brown, T.A., Ringrose, A.E., Cabedo-Sanz, P., Mundy, C.J., Gosselin, M., Poulin, M., 2013. Quantitative measurement of the sea ice diatom biomarker IP25 and sterols in Arctic sea ice and underlying sediments: Further considerations for palaeo sea ice reconstruction. Organic Geochemistry 62, 33-45.

Blaauw, M., Christen, J.A., 2011. Flexible Paleoclimate Age-Depth Models Using an Autoregressive Gamma Process. Bayesian Analysis 6, 457-474.

Blaauw, M., Christen, J.A., 2016. Bacon manual- v2.2.ed, 11 pp..

Blott, S.J., Pye, K., 2001. GRADISTAT: A grain size distribution and statistics package for the analysis of unconsolidated sediments. Earth Surface Processes and Landforms 26, 1237-1248.

Eberl, D.D., 2003. User guide to RockJock: A program for determining quantitative mineralogy from X-ray diffraction data. United States Geological Survey, Open File Report 03-78, 40 pp, Washington, DC.

Hunt, J.B., Hill, P.G., 1996. An Inter-Laboratory comparison of the electron probe microanalysis of glass geochemistry. Quaternary International 34-36, 229-241.

Jennings, A.E., Helgadottir, 1994. Foraminiferal assemblages from the fjords and shelf of Eastern Greenland. Journal Foraminiferal Research 24, 123-144.

Jennings, A.E., Weiner, N.J., Helgadottir, G., Andrews, J.T., 2004. Modern foraminiferal faunas of the Southwest to Northern Iceland shelf: Oceanographic and environmental controls. Journal of Foraminiferal Research 34, 180-207.

Olafsdottir, S., 2004. Currents and climate on the northwest shelf of Iceland during the deglaciation: high-resolution foraminiferal research, Department of Geosciences. University of Iceland, Reykjavik, p. 117.

Rytter, F., Knudsen, K.-L., Seidenkrantz, M.-S., Eiriksson, J., 2002. Modern distribution on benthic foraminifera on the North Icelandic shelf and slope. Journal of Foraminferal Research 32, 217-244.

Weltje, G.J., Prins, M.A., 2003. Muddled or mixed? Inferring palaeoclimate from size distributions of deep-sea clastics. Sedimentary Geology 162, 39-62.

Weltje, G.J., Prins, M.A., 2007. Genetically meaningful decomposition of grain-size distributions. Sedimentary Geology 202, 409-424.

Suppl. Table 1

Core	Number Fig. 8	Depth	P or B	14C date	error
ICELAND					
HM107-05	1	381	P	14100	140
	2	394	B	13690	100
	3	394	SHELL	13980	90
B997-326PC		18	B	9040	110
		111	B	9580	100
		125	Vedde/Saks		
	4	182	P&B	13835	215
		198	B	23570	340
B997-323		48	Vedde?		
	5	59	B	13100	130
	6	71		13400	190
		90	B	>25,00	
B997-338		21	B	11560	170
			tephra		
	7	98.5		13020	220
	8	193	shell	13507	78
		198	tephra		
	9	210	shell	13235	62
		319.5	B	31900	1700
		412	B	34600	640
MD99-2264			Vedde		
	10	1169	shell	11170	90
	11	1339	shell	12080	800
	12	1705	shell	12714	86
	13	2183	shell	13130	91
	14	2749	shell	13469	89
		37010	shell	53436	800
JM96-1234		349	B	14030	70
B997-336		501	shell	13680	70
HU90030-006LCF	15	1175	B	12690	195
	16	1235	B	12810	205
	17 CC		B	13105	85
MD99-2256	18	1184	shell	11840	90
MD99-2259	19	2048	B	12790	120
E. GREENLAND	20	2261	shell	13790	80
HU93030-007PC	21	7.5	P--Nps	15270	120

MD99-2260	22		11	P--Nps	16230	150
JM96-1216/2			55	BF	8180	80
			95	BF	9580	100
	23		210	shell	10625	90
	24		246	shell	12040	80
	25			BF	14450	150
BS1191-K18B			4.5		1680	50
			37		5215	75
			62		9292	80
			77		9240	90
	26		97	B	12325	80
	27	>150		N p s	12470	205
	28			N p s	12085	115
	29			B	12865	305
PO175/1-5			29.5	P & B	13100	110
	30		59.5	P & B	11995	145
			95	B	13300	145
	31		125	shell	13024	120
	32		194	B	14465	200
	33		311	B	14845	190
JM96-1213			100		Vedde	
			199	Triboculina	14680	170
	34		320.5	Bryozoa	12630	80
	35		389	B	13690	230
	36		439	N labradorica	13356	108
	37		473	Ex. Clavata	13830	270
MD99-2317	38		1851	Ex. Clavata	11567	88
	39		1982	bryozoa	11950	110
MD99-2322			2436	shell	10442	82
JM96-1214	40		562	B	11380	80
	41		469	Bryozoa	12700	110
JM96-1215	42		495	P & B	12260	100
	43	>587		B	12900	50
JM96-1225			47.5	P	12455	65
			52.5	18O transition		
			57	P	15380	130
JM96-1228			213	P	15140	185
			220	18O transition		
			231	P	16270	160

B = benthic forams

P = planktonic forams

deltaR = 0 fro to	range	Median	error	linear est deltaR	error
17000	16145	855	16544	222	1000	200
16265	15684	581	15974	150	906	200
16680	16070	610	16361	151	994	200
10362	9236	1126	9786	280		
11067	9878	1189	10458	290		
		0				
16891	15557	1334	16176	324		
27954	26660	1294	27420	307	3900	
		0				
15581	14438	1143	15072	271		
16154	15014	1140	15553	288	818	
		0				
13349	12698	651	13032	170	261	100
		0				
15636	14108	1528	14877	403	703	200
15993	15384	609	15715	151	851	200
		0				
15568	15114	454	15296	117	768	200
40848	32665	8183	36092	2073		
40226	36889	3337	38698	825		
		0				
12854	12538	316	12673	78	142	200
16346	11801	4545	13860	1122	418	200
14778	13997	781	14317	209	610	200
15479	14750	729	15152	172	736	200
15952	15316	636	15650	163	839	200
16704	16182	522	16423	131	1000	200
16192	15736	456	15962	116	900	200
15091	13815	1276	14379	345	603	
15231	13918	1313	14558	354	639	
15388	14724	664	15114	165	730	200
13481	13131	350	13309	88	346	
15037	14068	969	14494	261	633	
16340	15834	506	16105	126	936	
18394	17789	605	18087	151	1384	200

19496	18791	705	19106	183	1675	200
8951	8481	470	8689	122		
10683	10215	468	10447	125		
12382	11464	918	11944	212	-23	
13697	13316	381	13488	97	406	200
		0			1136	200
1337	1128	209	1238	50		100
5755	5392	363	5576	86		100
10318	9850	468	10109	114		100
10239	9732	507	100031	131		100
14010	13568	442	13795	108	492	200
14792	13464	1328	14003	335	536	200
13806	13311	495	13545	127	420	200
15163	14094	1069	14623	296	656	200
		0				
15537	14563	974	15089	226	727	200
13785	13185	600	13460	152	392	
15906	14975	931	15420	231	788	200
15709	14826	883	15267	215	704	200
17633	16458	1175	17078	299	1141	200
18043	17074	969	17589	247	1256	200
		0				
		0			1206	200
14554	13885	669	14139	163	585	200
16642	15268	1374	15965	344	906	200
15829	15163	666	15489	173	805	200
16985	15355	1630	16175	406	948	200
13250	12815	435	13042	109	263	200
13667	13196	471	13407	115	379	200
11915	11250	665	11571	179	-78	200
13055	12671	384	12845	98	206	200
14862	13938	924	14320	242	606	200
13961	13470	491	13718	125	473	200
15052	14313	739	14720	196	667	200
14107	13770	337	13937	86	532	200
		0	16180			
18529	17900	629	18205	160	1420	200
18387	17494	893	17936	227	871	200
		0				
19547	18810	737	19153	194	1690	200

from	to	Range	Median	error		Iceland
15741	14165	1576	15021	417		
15230	13844	1386	14523	373		
15569	14068	1501	14813	393		
10362	9236	1126	9786	280		
11067	9878	1189	10458	290		
		0		100		
161230	13561	147669	14797	667		
		0				
		0	12100			
14756	13344	1412	13918	354		
		0				
		0				
13313	12611	702	12949	186		
		0				
14875	13195	1680	13850	420		
15097	13727	1370	14327	365		
		0			14	
14751	13437	1314	13982	328		average
		0				median
		0				
		0	12100	100		
13026	11835	1191	12502	298		
15815	11150	4665	13314	1172		
14034	13134	900	13568	228		
14655	13365	1290	13891	317		
15091	13695	1396	14298	370		
15610	14119	1491	14888	393		
15196	13865	1331	14513	359		
14210	12915	1295	13575	320		E Greenland
14511	12996	1515	13667	354		
14605	13348	1257	13870	306		
13375	12596	779	12977	206		
14143	13146	997	13633	257		
15295	13924	1371	14615	367		
16984	15564	1420	16246	350		

17862	16460	1402	17190	354	
		0			
		0			
		0			
13485	12675	810	13098	209	
16156	14405	1751	15405	428	
1471	981	490	1229	119	
5859	5305	554	5576	143	
10434	9687	747	10087	184	
10366	9608	758	10013	188	
13749	12830	919	13297	226	
14012	12794	1218	13413	309	
13559	12670	889	13129	226	
14956	12946	2010	13795	495	
		0			
14637	13343	1294	13871	317	average
		0			
14991	13466	1525	14095	397	median
14647	13269	1378	13818	336	
16221	14303	1918	15410	478	
16685	14971	1714	15810	421	
		0	12100	100	
16447	14742	1705	15642	411	
13986	13090	896	13519	224	
15531	13675	1856	14550	474	
14993	13535	1458	14144	377	
15755	13736	2019	14688	523	
13164	12094	1070	12701	263	
13453	12629	824	13043	216	
		0			
13130	12060	1070	12667	267	
14065	13112	953	13570	241	
13708	12772	936	13250	231	
14150	13271	879	13701	231	
13836	12936	900	13391	221	
		0			
17080	15670	1410	16356	355	
17556	16040	1516	16794	390	
		0			
17897	16478	1419	17223	360	

from	to	median cal		
14605	13348	13870		16544
15741	14165	15021		15974
15230	13844	14523		16361
16230	13561	14797		15072
14756	13344	13918		15553
13313	12611	12949		14877
14875	13195	13850		15715
15097	13727	14327		15296
13026	11835	12502		14317
15815	11150	13314		15152
14034	13134	13568		15650
14655	13365	13891		14379
14210	12915	13575		15114
14511	12996	13667		13309
13375	12596	12977		14494
14143	13146	13633		16105
15295	13924	14615		
14644	**13094**	**13820**		
14706	13171	13759		15224

from	to	median cal		
13485	12675	13098		
16156	14405	15405		
13749	12830	13297		
14012	12794	13413		14623
14637	13343	13871		15420

14991	13466	14095	15267
14647	13269	13818	17078
16221	14303	15410	17589
16685	14971	15810	14139
13986	13090	13519	15965
15531	13675	14550	15489
14993	13535	14144	16175
15755	13736	14688	14320
13164	12094	12701	13718
13453	12629	13043	14720
13130	12060	12667	13937
14065	13112	13570	
13708	12772	13250	15264.6154
14150	13271	13701	13.9-14.2
14554	**13265**	**13897**	
14150	13269	13701	

Suppl. Table 2

		SiO2	TiO2	2O3	FeO*	MnO
Lipari obsidian standard	Mean	74.12	0.07	12.98	1.67	0.07
CU Lab n = 10	sd	0.86	0.03	0.41	0.21	0.02
B99-338						
90 cm	Mean	78.8	0.2	13.1	3.3	0.1
n = 3	SD	0.5	0.0	0.3	0.1	0.0
99-101 cm	Mean	74.0	0.3	14.0	3.8	0.1
n = 9	SD	4.8	0.1	1.9	0.7	0.0
190 cm	Mean	74.0	0.3	14.0	3.8	0.1
n = 9	SD	4.8	0.1	1.9	0.7	0.0
192-194 cm	Mean	77.1	0.3	11.7	5.7	0.1
n = 9	SD	1.5	0.2	1.4	2.4	0.1
Borrobol type	Lind et al 2016--Table 2 Mean	76.67	0.13	12.71	1.56	0.04
n = 10	standard deviation	0.35	0.01	0.25	0.17	0.01
	Similaritycoefficent					
	Borrobol v 90 cm	0.997				
	Borrobol v 100 cm	0.742				
	Borrobol v 90 cm	0.742				
	Borrobol v 193 cm	0.830				
	Basalt tephras					
B997-326	156 cm	49.18	0.53	14.18	8.42	0.17
B997-323	69 cm mean	50.04	2.20	13.16	12.96	0.23
	sd	0.64	0.47	0.56	0.89	0.02
	94 cm mean	50.68	3.35	13.28	13.69	0.24
	sd	1.56	1.01	1.26	1.33	0.03

MgO	CaO	Na2O	k2O	P2O3	Total
0.04	0.77	3.74	5.03	0.01	98.48
0.01	0.11	0.16	0.25	0.02	
0.0	0.5	1.4	3.0	0.0	100.2
0.0	0.0	0.5	0.3	0.0	
0.1	1.1	2.4	3.4	0.0	99.2
0.2	0.9	1.4	0.8	0.0	
0.1	1.1	2.4	3.4	0.0	99.2
0.2	0.9	1.4	0.8	0.0	
0.0	0.4	1.4	3.1	0.0	99.8
0.0	0.0	0.5	0.6	0.0	
0.08	0.75	4.03	4.01	0.01	
0.02	0.06	0.47	0.12	0.01	
10.28	15.76	1.39	0.04	0.05	100.00
6.95	10.96	2.47	0.21	0.28	99.47
0.60	0.44	0.21	0.06	0.29	0.83
5.38	9.40	2.86	0.57	0.38	99.83
1.54	1.54	0.56	0.41	0.16	1.25

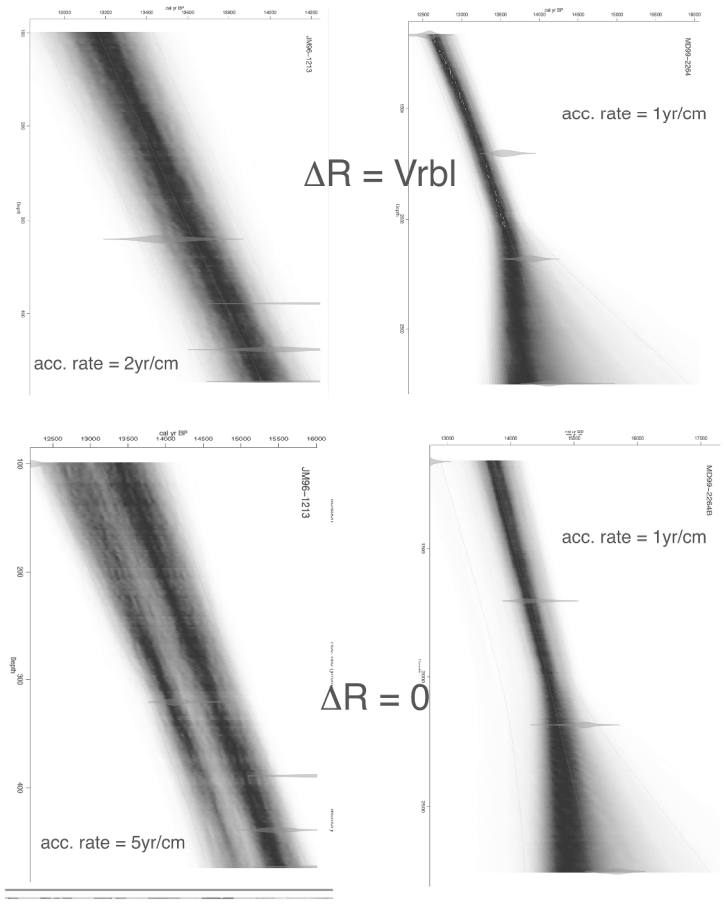

279x361mm (300 x 300 DPI)

PO175/1-2

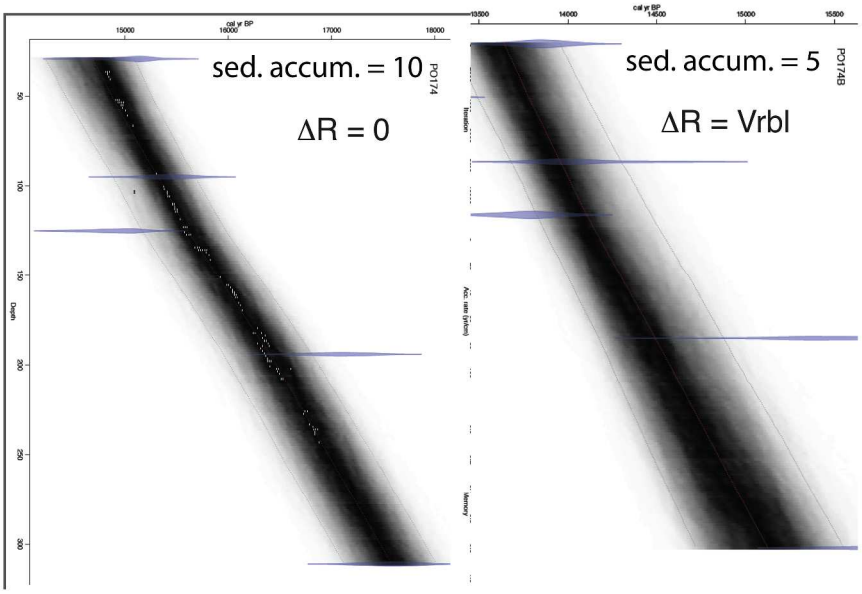

330x408mm (300 x 300 DPI)